# An experimental preparation to monitor neural signals in the visual thalamus of awake behaving mice

*Daniel Borisov*

Department of Physiology

McGill University, Montreal

August 2020

A thesis submitted to McGill University in partial fulfillment of the requirements of the degree of Master of Science.

# Table of Contents

# I. Abstract

Behavioral responses are strongly influenced by the location of visual stimuli –the brain 'sees' a large object moving overhead as a threat quicker than it can detect the same object on the ground. In mice, the retina represents stimuli from all points in space equally, suggesting that the location-dependent difference in feature selectivity arises downstream. Recent results indicate that LGN responses to such stimuli vary in strength depending on retinotopic location. To determine how this non-uniformity arises we developed a procedure to allow for the investigation of these phenomena. We designed and built a custom two-photon microscope (2p), infected mouse LGN with regular GCamP6f and axon-localized GCamP6s and imaged the responses of both LGN cell bodies through a cannula, as well as LGN neuron terminals in V1 through a cranial window. Initial mapping using epifluorescent imaging showed clear retinotopic maps and responsiveness to a moving bar motion stimulus. By comparing neural responses evoked by such stimuli, this procedure can be used to map the distribution of feature selectivity in LGN bodies as well as their inputs to V1.

## II. Résumé

Les réactions comportementales sont fortement dépendantes de l'emplacement d'un stimulus visuel – le cerveau « perçois » un objet s'approchant du ciel plus rapidement qu'un objet provenant du sol. Toutefois, la rétine d'une souris représente les signaux visuels de façon équilibré à travers tout le champ visuel, suggérant que ces différences comportementales spatio-dépendantes surgissent en aval. Des études récentes indiquent que le LGN varie sa réaction aux stimuli visuels en fonction de leur emplacement rétinotopique. Afin de comprendre comment ces réactions non-uniformes surgissent, nous avons développé une procédure pour investiguer ce phénomène. Nous avons conçu et construit un microscope biphoton (2p), infecté le LGN de souris avec un virus GCamP6f typique ou une variante localisée à l'axone et imagé les réponses calciques du LGN en observant soit les corps cellulaires du LGN à l'aide d'une canule ou les projections situées dans le cortex V1 avec une fenêtre crânienne. L'imagerie à l'épifluorescence démontre une carte rétinotopique claire en utilisant un stimulus de barre mobile. En comparant les réponses neurologiques induit par des stimuli variés, cette procédure peut être utilisée pour schématiser la distribution spatiale des représentations de traits visuels dans le LGN et leurs projections dans V1.

## III. Acknowledgements

My graduate studies would not have been possible without the aid of many great people. Most importantly, I want to acknowledge my supervisor, Dr. Arjun Krishnaswamy, who helped me develop and improve on the many skills required to do good science, such as critical thinking, presentation, experimental design, and scientific writing skills, and provided editorial help with my written communications and thesis. When things went well, he was encouraging and when they weren't, he was patient, and was critical for my development as both a scientist and as a person. I would also like to acknowledge his support in the construction of the two-photon imaging apparatus, and material preparations through viral injections and surgical procedures. I would also like to acknowledge my committee members, Erik Cook, Stuart Trenholm, and Adrien Peyrache, for their comments, criticisms, and ideas that helped me refine my research. I would especially like to acknowledge Erik Cook for his assistance with the development of the stimulus control system used in the experimental procedures and help with the time synchronization analysis.

I would like to acknowledge my fellow students, Pierre-Luc Rochon, Aline Giselle Rangel Olguin, and Jonas Lehnert, for their support and help in making my progress possible. Specifically, I would like to thank Pierre for the tutoring he provided that helped me develop the wet lab skills needed to be successful in my work, as well as the constant constructive ideas he provided. I would like to thank Aline for her help in providing confocal imaging support. I would like to thank all of them for making my time in the lab a pleasant experience.

I would like to acknowledge the lab technicians, Monika Noble, Joellyne Evaristo, and Catherine Theriault, for providing assistance in the preparation of materials for the experiments, and more specifically Catherine for her viral injections, and Monika and Joellyne for their viral injections and cranial window preparations.

## IV. Contribution of Authors

The thesis was written by the author, with thematic guidance and editorial support provided by Dr. Arjun Krishnaswamy, and French translation services by Pierre-Luc Rochon. The author contributed to the development of the surgical procedures, assisted in the design of the imaging apparatus, performed the imaging experiments, performed data analysis, and designed the figures.

# 1 Introduction

Our abilities depend critically on the way the brain encodes information. In vision, this process begins in the retina when light strikes the photoreceptors. These photon signals are then analyzed by ~ 30 types of retinal ganglion cells (RGCs). Each RGC encodes an aspect of the visual world, such as color or motion, and relays this message to the brain[1,2]. The dorsal lateral geniculate nucleus of the thalamus (LGN) offers a tractable model to determine how the brain uses the retinal message to create sight. Located one synapse from the eye, LGN receives direct input from RGCs, whose axons organize themselves across LGN according to RGC soma location in the retina, a phenomenon called retinotopy[1,2]. Neighboring LGN neurons therefore relay retinal input from neighboring points in visual space to visual cortex. Recent studies suggest this view is too simple – feature responses in LGN are found in discrete regions even though corresponding RGC projections are widespread[3–5].

The implication is that the LGN might be a processing region that modifies the incoming retinal signal before sending it to the primary visual cortex. While many of the retinorecipient regions of the brain are responsible for reflexive, non-imaging forming processing, the LGN represents the represents the primary route of visual information to cortex. Thus, if this view is correct, then the localized LGN feature representations should carry a functional and behavioural relevance to cortical visual processing. Furthermore, if local geniculate processing was responsible for these non-uniform regions, then it is possible these representations are plastic, and could be modified through learned behaviours or attentional training.

We hypothesize that the LGN amplifies feature signals being received from the eye to support behavioral performance. If true, then we would expect that:1) Feature preference varies non-uniformly over the LGN despite a uniformity of feature input; 2) Such non-uniform maps of

visual features results from local geniculate processing; and 3) Behavioural performance to feature-based visual tasks should vary based on variations in feature processing in these localized regions, as induced through natural feature presentation or through artificially induced perturbations.

The goal for my master's thesis was to develop an experimental preparation which would allow testing of these ideas. Below, I review some basic aspects of retinal and visual circuitry, the wiring and anatomy of the LGN, and the function of this structure in the context of passive and active viewing.

## 1.1 The Early Visual System

Vision begins in the eye, an optical organ that utilizes an organic lens to direct incoming electromagnetic radiation towards a thin sheet of neural tissue at the back of the eye called the retina. The retina is a neural system that is composed of multiple cell types: photoreceptors, interneurons, projection neurons, and Muller glia[6]. This neural system is well-organized and structurally layered in a way that is representative of the directional flow of information[6].

### 1.1.1 Photoreceptors

Light detection in the retina begins when the incoming photons strike the photoreceptors, are absorbed by the photopigment rhodopsin, and initiate a series of second messenger cascades that amplify this signal and transduce it to a change in photoreceptor membrane voltage[7]. Two distinct class of photoreceptors exist: cones and rods, each of which allows for vision at different illumination levels. Rods are sensitive photoreceptors that are ideal in low-light environments, detecting individual photons, while cones are optimized for daylight illumination levels[8]. Furthermore, variation in cone opsin structure allows for optimal photon absorption at different wavelengths, providing the basis for colour vision. In the average human retina, three cone types

(S, M, and L) exist which are tuned to the 420 nm, 450 nm, and 620 nm wavelengths, and the relative activation allows for hue differentiation in humans[9]. Mutations in human genes encoding for cone photopigments carry clinical significance in cases of colour blindness (dichromacy) while other cases carry the potential for human female tetrachromacy due to their dual X-linked photoreceptor genes[10,11]. Once a photon has been absorbed by a photoreceptor, the signal is propagated along the cell and transmitted through its synapse to a bipolar cell.

### 1.1.2 Interneurons: Horizontal, Bipolar, and Amacrine Cells

The photoreceptors synapse onto bipolar cells and are depolarized in the dark, constantly releasing glutamate and are hyperpolarized when exposed to light in graded fashion[7]. Release is initiated by voltage-gated L-type calcium permeable channels on the presynaptic membrane, channels that are closely related to the L-type calcium channels found on cardiomyocytes[12]. Steady release is mediated by the presence of a synaptic ribbon, which suspends synaptic vesicles above the presynaptic active zone and acts like a conveyer belt that can fuse vesicles with the terminal membrane[13]. Furthermore, this release is constantly being modulated by horizontal cells, and while the mechanisms through which it does this are still unknown, some current theories suggest that it occurs through mechanisms involving GABA and nitric oxide feedback, glutamate autoreception, and amacrine dopamine release, with the modulation generally thought to act as a gain control mechanism[14–20]. Owing to their large lateral spread and gain control functions, the horizontal cells are thus thought to help photoreceptors adapt to different environmental illumination levels.

The bipolar cells are the principle targets of the photoreceptor signal and represent the first stage of visual signal processing. In mice, there are 11 cone bipolar cell types and 1 rod bipolar cell type, with each cone photoreceptor synapsing onto one of each of the cone bipolar cell types[21]. These different bipolar cell types correspond to different feature encodings, such as the on and off

responses that are mediated by different glutamate receptor expression[22–25]. The cone bipolar cells then project their signals down onto retinal ganglion cells. Rod bipolar cells, on the other hand, project onto dopamine modulated amacrine cells that excite ON-cone bipolar cells via gap junctions and inhibit OFF-cone bipolar cells via glycinergic synapses. The rod signal thereby hijacks the cone signaling pathway[26]. The bipolar cell projections stratify in 5 distinct sublayers of a specialized neuropil called the inner plexiform layer. The stratification provides functional separation of the incoming signal into ON signal layers and OFF signal layers[27], though exceptions to this rule exist in some cell types[28,29]. Furthermore, the stratification also provides functional separation for directionally selective cells into the ON DS layer, OFF DS layer, or both for ON-OFF direction selectivity[30–32].

The final interneuron type found in the retinal structure is the amacrine cell. Amacrine cells are extremely diverse, with at least 26 different identified amacrine cell types varying in morphology and layer stratification, and could range up to a potential 60 different amacrine cell types[33,34]. The diversity of amacrine cell types corresponds to a variance of function, such as developmental retinal circuit refinement[35], rod signal processing[36], motion-direction processing[37], and diffuse modulation[38], among other unnoted and potentially undiscovered functions[34].

### 1.1.3 Retinal Ganglion Cells

Retinal ganglion cells (RGC) are the final processing units found in the retina and are the projection neurons that send the visual signal from the eye to the brain. RGCs integrate signals from bipolar and amacrine cells and send this information to their retinorecipient targets. Up to 40 different types of retinal ganglion cells have been identified, with different RGC types being attuned to different aspects of the visual scene[39]. Some RGC types correspond to visual features, such as suppressed-by-contrast RGCs[40], while others correspond to motion detectors, such as an

RGC type that serves as a differential motion detector[41]. As a result, the signal that the RGCs send to the brain from the eye is comprised of up to 40 parallel feature representations of the visual scene, and is a complex processed signal, rather than a simple camera-model pixel representation of the world.

### 1.1.4 The Visual Pathway

As RGC axons leave the eye and begin their path to the brain, a subset cross from one side of the brain to the other. This crossing occurs at the optic chiasm, and as a result the visual signal for one visual field is processed contralaterally in the brain[42]. Anatomically, this crossing is inconsistent across mammals[43]. Primates have an almost 50% nasal-temporal split across the retina, with the nasal half of the cells projecting contralaterally, and the other half projecting ipsilaterally[44]. The result is that the primate brain processes the contralateral visual field with large binocularity. Mouse retinas, on the other hand, maintain contralateral projections from across the entire retina, with a small ventro-temporal crescent-shaped area of the retina that has some ipsilaterally projecting ganglion cells[45].

Once the axons pass through the chiasm, they are sent to different regions of the brain. In fact, there appear to be 46 different subcortical retinorecipient regions in the mouse brain[46]. As a result, it becomes a challenge to broadly discuss the concept of vision beyond the retina and understanding what the brain does with the visual signal coming from the eye, and the functional relevance of each individual signal, becomes difficult to discern. However, only one of these subcortical regions has a direct projection to the primary visual cortex (V1) and is therefore considered the main image-forming pathway from the eye, a region called the lateral geniculate nucleus of the thalamus (LGN). Therefore, understanding how this region works is fundamental to understanding visual cognition in higher order visual processing centers.

### 1.1.5 Lateral Geniculate Nucleus of the Thalamus

The LGN is the sole source of visual input to V1. Classically viewed as a simple relay between the retina and V1, new results show that processing occurs at LGN before the signal is relayed[47]. In many diural mammals, including primates, the LGN is a layered structure containing three distinct layers: the parvocellular layer, the magnocellular layer, and the koniocellular layer[48–50]. Each layers receives input from a distinct set of RGCs, and each layer maintains different receptive field properties[51–56]. Furthermore, each layer projects to a distinct section of V1 or extrastriate area, and thus represents a parallel pathway for the visual processing that is sent to the visual cortex[57–59] (for a more detailed discussion refer to §1.6.3 Relay Outputs).

Although the main function of the LGN is to relay the retinal signal to V1, retinal synapses only account for roughly 7% of the total incoming input; the rest are synapses from various regions of the brain[60]. A complete understanding of how cortical processing works will require an understanding of how LGN processes the incoming visual signal, how its output is modulated according to non-retinal inputs, and the behavioural relevance of these modulations.

### 1.1.6 Superior Colliculus

Another important retinorecipient region in the early visual system is the superior colliculus (SC). The SC has been extensively studied, and its role in saccade generation and control is well documented, and their different cell type properties characterized. It was found that rostral SC firing can suppress spontaneous saccade generation and allow for visual fixation, while firing in the foveal retinotopic region of the SC induced microsaccade generation[61–63]. However, the SC also represents an important region for cortical processing of the visual signal, as it projects to extrastriate areas through the pulvinar[64], and through this pathway plays an important role in the phenomenon of blindsight[65]. Interestingly, SC projects to the LGN, and its synapses have the

capability to drive LGN spikes, suggesting particularly strong tectal control of thalamocortical signaling[66,67].

## 1.2 *Mus musculus* as a Model for Vision

*Claude Shannon's* information theory[68], and more specifically his conceptualization of a communication system, has previously been used to try and understand neural processing[69,70]. In systems theory, the black box model allows an investigator to understand a system by characterizing its inputs and outputs, and recursively applying the model to the internal elements of the black box as a way to fully define the system under study. Applying the black box model to neural communication systems provides a method to allow neuroscience researchers a way to gain an understanding of the brain. As a result, this characterization model requires three fundamental pieces: the ability to control the inputs, the ability to measure its outputs, and access to its internal elements to apply the method recursively. While understanding the human visual system would provide the most relevance from an applied sciences perspective, human subjects pose a logistical challenge due to the invasive procedures required to probe the internal elements of the visual system black box. As a result, extrapolating from animal models can provide an opportunity to gain insight into human neural processing, and finding the best animal model becomes a balance of obtaining a representative approximation of the human visual system while providing a way to apply the three key pieces required for systems analysis.

Several animal models have been studied to help approximate and understand the function of the human LGN, including non-human primates such as the macaque[71] and marmoset[72], cats[73], and squirrels[74]. Using the mouse (*Mus musculus*) as a model for vision has recently become accepted as a viable solution for answering many of the questions required to obtain a thorough understanding of neural image processing.

### 1.2.1 Advantages of the Mouse Model

Mice offer several advantages for the study of vision. First, the average mouse reaches sexual maturity at 6-8 weeks of age, has a 6-month reproductive life span, 20-day gestation period, produce 4-12 pups per litter, and are weaned at 4 weeks of age, making them an abundant resource for scientific methodology. This rapid breeding cycle offers significant advantages for genetic manipulation.

The prevalence of the transgenic mouse has proved useful for understanding the elements of the visual system. Current mouse lines allow one to mark, monitor, and manipulate many neural cell types in a variety of brain structures. The general scheme in such approaches begins with the identification of a gene uniquely labeling a neural subset of interest to allow for the exploitation of these cell subsets. These genes can either be interrupted through the addition of a construct bearing a DNA nuclease (such as Cre-recombinase), or can have the construct appended, providing expression of both proteins. The result is a Cre-line that can be crossed to a mouse bearing a fluorescent reporter whose expression depends on the excision of a STOP cassette. The outcome is that cells expressing the nuclease have the cassette excised, allowing for the production of the fluorescent reporter, creating a fluorescently labelled cell[75].

Variations of this technique in which the fluorescent reporter gene is changed allows for the introduction of light activated ion channels such as channelrhodopsin-2[76], chemogenetic activators or silencers such as designer receptors exclusively activated by designer drugs (DREADDs)[77], or genetically encoded calcium indicators (GECIs) such as GCamP6[78]. These variations offer easy routes for assessing neuronal structure and function. An alternate route delivers the nuclease-dependant construct as a virus and shortens the time needed to obtain experimental reagents at the cost of the total number of neural types transduced.

The genetic tools afforded by the mouse provide a way to probe the internal elements of the visual system of the mouse using specific protein types. Specifically, the targeted expression of optical indicators, optogenetic neural control, and designer receptors can allow for both recording and control of neural elements. Optical indicators such as the calcium indicators GCamP6[78] or voltage indicators such as Ace-mScarlet[79] coupled with two photon imaging of a large field of view allows for many single-neuron recordings to be acquired simultaneously, offering an advantage over conventional neural recording methods that could only measure either individual or small groups of neurons. Similarly optogenetic methods[80,81] and genetically encoded DREADDs[77] allow for selectively perturbing the activity of a large number of neurons. Coupled with the smaller size of mouse cortical regions and their lack of cortical folds, it becomes possible to record from neurons in entire regions simultaneously, an advantaged conferred to mice that would not be possible with other animal models.

Similarly, visual input can be easily controlled using monitors or projectors, and behavioural output recorded using behavioural tasks such a running wheel or lick spout[82,83]. Therefore, given the tools available to control its inputs, measure its outputs, and probe its internal elements, the mouse presents an ideal mammalian model to study the visual system.

### 1.2.2 Comparison of Mouse and Human Vision

There are several differences between the mouse and human visual systems. Processing of vision in the mouse and human begins to diverge in the retina, at the photoreceptors. Humans and non-human primates utilise three cones types to process colour, utilising colour-opponency to differentiate between hues[9]. However, mice only have two cone types with sensitivities at 360 nm and 511 nm wavelengths, and each of these cones are distributed in different parts of the retina[84]. As a result, it is possible that mice might not have colour vision through cone colour-opponency,

though evidence exists for rod-cone opponency to allow for dichromatic hue differentiation in the mouse[85]. Mouse and human variance in photoreceptor topography are a major factor in the difference between vision in the two animals as well. Though humans and mice have a similar cone-rod ratio (97% for mice[86] and 95% for humans[87]), a major topographical difference between the two animals is the presence of the fovea in primates. The fovea represents a dense region of photoreceptors at the center of the visual field that is entirely devoid of rods and provides the greatest visual acuity. Though rods outnumber cones in the human retina, the foveal cone density is greater than the rod density in the human retina[87]. In contrast, the mouse retina lacks a foveal region, and rod density is approximately 30 times greater than cone density throughout the mouse retina[86]. Given that humans are diurnal mammals and are active during photopic conditions, while mice are crepuscular and nocturnal and are active during scotopic and mesopic conditions, the cone-dominant and rod-dominant vision differentiation has an ethological relevance.

Another important distinction that must be noted between the two animals is the anatomical organization of the LGN. While the primate LGN is laminated into its P, M, and K layers, the mouse LGN does not show such lamination patterns. However, the mouse LGN does contain three distinct relay cell architectures, the X, Y, and W cells, and maintains distinct feature-specific functional regions, each containing a full retinotopic field of view, and represents parallel processing pathways that, while not anatomically similar, maintain a functional similarity to the primate geniculate[2,88]. Further discussion of the LGN anatomical structure follows in § 1.6 Anatomical Wiring of the LGN.

## 1.3 Retinal Feature Detection

The retinal signal is composed of at least 40 parallel feature channels, each being encoded and projected by a unique retinal ganglion cell type[89]. The feature processing begins at the

photoreceptor-bipolar cell synapse, ends with RGC processing, and makes use of amacrine cells in the intermediary[6,34]. Understanding the feature processing in the retina is the first step to discovering the way the brain encodes visual information.

### 1.3.1 Contrast Detection

One of the very first feature processing steps that occurs in the retina is the separation of the photoreceptor signal into on and off feature channels by the bipolar cell types (refer to § 1.1.2 Interneurons: Horizontal, Bipolar, and Amacrine Cells for an explanation of the two signals and how they arise). These on and off projections of the bipolar cells are then sent to the inner plexiform layer, where they synapse with the retinal ganglion cells in functionally distinct lamination patterns. The two outer layers, and the outer part of layer 3, correspond to the OFF sublamina, while the inner part of layer 3, and the two inner layers, correspond to the ON sublamina, and response properties of ganglion cells with dendritic arbors in these layers respect this functional organization, including the bi-stratified ON-OFF RGCs[90,91].

Furthermore, various subsets of the standard ON and OFF response features are encoded in various RGC types. The alpha RGC is a well-studied class of RGC that has distinct morphological properties, presenting as monostratified RGC cell type with the largest soma and large dendritic arbors that can be found in the retina of many species[92]. These RGCs comprise a few subtypes that respond to either ON or OFF stimuli, with either sustained or transient responses [93]. These four ON and OFF retinal ganglion cell types are also joined by the ON-OFF transient RGC, a unique bi-stratified cell type with complex firing patterns[94].

### 1.3.2 Intrinsically Photosensitive and Suppressed-By-Contrast feature detectors

Alongside the classical center-surround RGCs that encode simple ON or OFF receptive fields are a variety of RGCs that encode for non-standard static features in the visual scene. One

such cell type is the melanopsin containing RGC, an RGC that does not require photoreceptor input to detect light, and is responsible for control of circadian rhythms in the brain[95]. These melanopsin-containing RGCs were also found to help drive pupillary responses, encode for a specific colour opponency, and potentially contribute to the image forming pathway through projections to the LGN[96–98]. Other unique feature-encoding RGC types are those that instead respond inversely to contrast. Two such types were noted as being either tonically or transiently suppressed by the presence of contrast[40]. Suppressed-by-contrast RGCs were also found to be spatially tuned when presented with a drifting grating, and the presence of an impressed-by-contrast RGC was also noted[99]. A bistratified RGC type was also discovered that encoded for feature uniformity in the visual scene and had transiently supressed firing patterns to both ON and OFF stimuli when a change in the scene had occurred[100].

### 1.3.3 Motion Detectors

Other important RGC types are those that encode for moving stimuli. Directionally selective RGCs (dsRGC) are a class of RGC types that respond strongest to a stimuli moving in its preferred direction (tuned to one of the four cardinal directions: nasal, temporal, ventral, or dorsal), and their weakest response to a stimuli moving in the opposite direction[101,102]. A large variety of motion-detecting functional RGC types have been documented, including the ON, OFF, and ON-OFF directionally selective RGCs (dsRGC)[89]. A cholinergic and GABAergic amacrine cell type, the starburst amacrine cell (SAC) was found to be necessary for direction-selectivity computation. The dsRGCs stratify in the cholinergic IPL bands with SACs and an asymmetric inhibition/excitation by SACs and bipolar cells are responsible for directionally selective computation, and it was shown that the loss of SACs leads to a loss of direction selectivity in dsRGCs[103–106].

## 1.4 Feature Detection in Striate Cortex

The very first striate recordings in by Hubel and Wiesel indicated early on that cortical receptive fields were not the same as the standard center-surround fields seen in the retina or LGN, and that they were instead tuned to bars or edges of a specific size and orientation, and often most responsive to a bar moving in a specific direction rather than a static one[107]. They then proposed the hypothesis that cortical receptive fields were novel, being computed through geniculate receptive field integration along a specific axis[108]. It became clear that feature detection in visual cortex was not simply inherited from the features computed in the retina, but rather created representations of the visual world through its own computations. Understanding which retinally-computed features are relevant for striate processing and which features are computed in the cortical regions de novo is a critical milestone in our understanding of sight.

### 1.4.1 Feature Computation

As Hubel and Wiesel first proposed[108], to detect edges and bars V1 has to compute new features from its simple inputs. Pyramidal neurons sum input from spatially offset and oppositely contrast tuned TC inputs. This offset occurs along a single axis, and the result is a grating-like receptive field with either a dark or bright receptive field center bounded by a surround of the opposite sign on either side. Furthermore, if silencing dsRGCs fails to silence V1 direction selectivity, then the cortical areas must be computing motion selectivity through the classical geniculate inputs as well. Initial theories proposed the idea of an intracortical inhibitory interneuron circuit to create a spatiotemporal offset in order to compute directional motion[109,110]. Supporting this idea was the finding that activation of local interneurons in V1 improved feature tuning for orientation and direction selectivity[111]. However, a recent study proposed that V1 direction selectivity could arise from simple summation of spatially offset transient and sustained

geniculate neurons, without the need for local interneurons to produce the required spatiotemporal offset[112]. Interestingly, many of the known cortical feature computations are already performed in the retina, raising the question of why V1 recomputes these properties. The answer to this question is still at large.

### 1.4.2 Feature Inheritance

Anatomical thalamocortical circuit tracing coupled with dsRGC retinogeniculate circuit tracing has shown that retinally computed direction selective features are relayed to layer 1 of V1, bypassing the dense thalamocortical layer 4 projections[113]. This retinal-geniculate-striate directionally selective pathway was shown to be functionally relevant, as a study looking at dsRGC ablated mice found that, while layer 2/3 V1 cells maintained their proportion of directionally selective cells, the cells lost a posterior motion tuning bias[114]. The implication is that while dsRGCs are not necessary for V1 direction tuning, they play an important role in inducing a tuning bias, specifically in the rostrolateral area[115]. These discoveries then lead to an important question: what is the functional or behavioural relevance of this tuning?

### 1.4.3 States and Learning

An important aspect of V1 is the modulation that occurs in response to behavioural states[116–123]. It was found that running and resting states in a mouse increased or decreased firing strength of visually stimulated V1 neurons respectively, while showing no change in geniculate signaling[116]. Further studies on running and resting states have implicated acetylcholine activations of the VIP GABAergic cortical neuron, causing disinhibition of a GABAergic somatostatin cell and resulting in increased V1 firing rates[117]. However this view is contested, and some evidence suggests the increases in firing rate are less general and are context-dependant[118]. The overall

implication is that higher order associations and states influence visual signal processing as early in the processing pathway as V1.

Furthermore, learning plays an important role in V1 processing. It was found that when undergoing a learning task, cortical neurons showed improvements in tuning for orientation discrimination, and that these visual improvements preceded behavioural improvements[119]. Additionally, it was found that the learning based changes in V1 are task-dependant and require task engagement in order for the changes to be observed[83].

### 1.4.4 Corticothalamic Feedback

Interestingly, LGN thalamocortical relay cells serve as the driving inputs to V1 while at the same time receiving feedback projections from layer 6 of V1. It was found that in primate V1 corticogeniculate feedback projections, receptive fields of the V1 neurons synapsed in their respective retinotopic locations within the LGN[124,125]. Cell recordings of LGN neurons in the presence or absence of V1 feedback, as controlled through V1 ablation, found that V1 strengthens LGN signaling when presented with a stimuli in its receptive field, and reduced LGN firing when a stimulus was presented outside of its classical receptive field[126]. V1 corticothalamic feedback to LGN thus acts as a gain control mechanism for presented stimuli, though to what purpose is yet to be fully determined. To fully understand how LGN signals are processed in V1 would require knowledge of how V1 signals are processed in LGN.

## 1.5 Geniculate Cell Types

While the classical view of the LGN has always been as a relay of the retinal signal to V1, the diversity of cell types paints a different picture. The LGN is made up of excitatory thalamocortical relay cells with varying different response properties, as well as different inhibitory interneurons. Glutamatergic thalamocortical relay cells are distinguishable by their

expression of the glutamate transporter subtype VGluT2[127], while the GABAergic inhibitory interneurons in the LGN are identifiable by their expression of the glutamic acid decarboxylase enzyme subtype GAD-67[128].

### 1.5.1 Excitatory Relay Cells

LGN relay cells exhibit three distinct morphologies, coined the X-like, Y-like, and W-like cells, and expression of these cell types is localized to certain regions in the LGN, yet no functional distinction between the cells has been found[88]. In fact, a connectomic analysis of relay cells found that cell morphology had no relevance to connectivity, and that relay cell classification was fuzzy, with the best classification based on RGC bouton size and perforation, and whether the boutons synapsed on dendritic spines or shafts[5]. An imaging study of mouse geniculate relay cells found localization of response properties for direction and axis selective relay cells, with horizontally preferring direction and axis selective cells located within the shell region of the LGN and vertically preferring direction and axis selective cells located within the LGN core[129]. Response properties of classical center-surround LGN relay cells have been characterized in a study utilising electrode recordings and the results published[130].

### 1.5.2 Inhibitory Interneurons

LGN inhibitory interneurons have been classified into two subsets, those found within the LGN and those found just outside in the perigeniculate region[131]. Within the intrageniculate inhibitory interneurons, staining has revealed two different cell types with differing morphologies and communication mechanisms, with some communications occurring through dendro-dendritic connections[132,133]. Perigeniculate interneurons appear to induce a generalized inhibition across the LGN, while intrageniculate interneurons maintain specific receptive fields, and are innervated by both RGCs and V1 feedback connections[131].

### 1.5.3 Serotonin and Acetylcholine

While the LGN is made up of excitatory and inhibitory cells, there is further diversity in the receptor expression within the LGN itself as well. LGN cells receive cholinergic and serotonergic inputs, modulating geniculate cell firing[134–136]. Furthermore, serotonergic innervation of LGN is not uniform, with densities varying throughout the LGN[137,138].

## 1.6 Anatomical Wiring of the LGN

Even though the geniculate relay is the only image forming pathway, only 5-10% of incoming afferents to the LGN are from RGCs[60], and only 80% of RGCs project to LGN[139]. Mapping the wiring of the LGN can provide insight into why not all of the RGCs are required for conscious vision, and how the many modulatory inputs affect visual behaviour.

### 1.6.1 Retinal Inputs

The retinal projections into LGN organize themselves in a retinotopic manner, projecting visual space as a map onto the LGN molecular gradients that pattern this structure during development[140,141]. Furthermore, while maintaining a functional retinotopic mapping, retinal inputs are segregated into different locations based on the RGC channel feature representation, with ON-OFF dsRGC projections into the shell region in the mouse LGN[32,142]. Interestingly, while RGC bouton representation appears to be diverse, uniform, and intermixed across retinotopic space in the LGN[4], the respective feature tuning of the geniculate neurons lacks this uniformity, producing regions with certain feature preferences relative to other areas[3].

### 1.6.2 Modulatory Inputs

Although retinal projections are the main drivers of thalamocortical relay cells in the LGN, their connections account for only a fraction of the synapses within this structure. Large numbers of synapses come from modulatory brain areas, indicating that the LGN may not just function as

a simple relay[143]. The reticular formation, a thalamic region associated with attention, acting as a thalamocortical gatekeeper[144], is one of the modulatory inputs to the LGN and has been shown to modulate geniculate firing rates based on whether attention is directed at or away from a specified stimulus[145]. The dorsal raphe, the serotonergic center of the brain, has been associated with various states such as sleep-wake cycles[146], reward[147], and satiety[148,149], and has serotonergic synapses in the LGN, which modulate visual activity[134]. Further modulatory input comes in the form of corticothalamic feedback from V1, where downstream activity feeds back, affecting its own input signals[126].

### 1.6.3 Relay Outputs

LGN thalamocortical relay cells transmit the visual signal to the primary visual cortex. While the majority of efferents project to layer 4 of cortex, LGN axons can be found within all layers of cortex, with segregation among parallel channels. It has been shown that geniculate relay cells target a variety of different pyramidal and stellate cells, causing both excitatory and inhibitory activation within primary visual cortex[150]. Furthermore, mouse LGN studies showed that directionally selective and orientationally selective LGN efferents project to layer 1 of visual cortex[113,151]. Furthermore, various studies show that some LGN axons bypass V1, connecting directly to extrastriate areas[59,152,153]. Interestingly, a macaque study found that parvocellular efferents project to layers 2/3, 4A, 4Cb, and 5, while magnocellular efferents project to layers 4Ca, 4Cb, and 6, resulting in a parvocellular pathway to V2 and a magnocellular pathway to area MT of cortex[154].

## 1.7 Function of the LGN

The LGN serves as a gateway for the retinal signal to reach the striate cortex. While its primary function is to relay the visual signal, the diversity of its wiring patterns means there is a lot more than meets the eye when understanding geniculate function.

### 1.7.1 Feedback Control

Given that the retina only contains outgoing projections, the LGN provides the first point of contact for any visual cortical feedback. Therefore, as a visual relay, the LGN is positioned as a nucleus that offers the cortex the ability to modulate its own visual input before it is received. Various studies looking at corticothalamic feedback to LGN have shown that cortical modulation can manipulate the geniculate signal[124–126]. If V1 received inputs directly from the retina, without the geniculate to act as a relay, the cortex would lose its opportunity to condition the incoming visual signal.

### 1.7.2 States

The LGN receives modulatory inputs from various brain regions responsible for state control and attention, such as the dorsal raphe and reticular formation[134,145]. As a result, the LGN provides a gated relay to the visual cortex that can be modified by the internal states of the animal and can modify the image-forming pathway before the image is even formed. The LGN could therefore play an important role for selective visual attention and play a behaviourally relevant role in visual processing.

Many of the studies investigating states and vision have utilised anesthetised mice, yet it has been shown that anaesthesia has an effect on thalamocortical relay cell channels and can affect spiking properties[155]. As a result, to study the mouse visual system and understand the role of the LGN in visual processing, utilising awake behaving animals becomes a necessity to understand

the behavioural effects related to states and the way its processing might be dynamically altered to suit behaviour.

# 2 Methods

## 2.1 LGN Surgical Procedure

### 2.1.1 Viral Injections

The calcium indicator GCamP6f was used to allow for LGN cell body imaging to measure responses. Expression was induced through a viral delivery using retrograde AAV carrying the GCamP6f DNA injected into V1 of the mouse (Figure 1a).

Isoflurane in balance oxygen was used for anesthetic initiation (5%) and maintenance (1.5-2.5%) of the mice. Once anesthetized, the mouse was given a 20 mg/kg injection of carprofen subcutaneously. Systane eye lubricant was applied to the eyes of the mouse. The fur on the scalp was shaved using a trimmer and the scalp was cleaned three times with 70% ethanol and 0.2% Chlorhexidine Gluconate. Once sterile, an incision 1 cm in length was made using a #15 scalpel. 50 µL of a lidocaine/bupivacaine mixture was injected onto the incision site. A microinjector was positioned for an injection into the left V1 (2.35mm lateral and 2.85mm posterior to the Bregma suture). A dental drill with bit an FG 4 bit was used to thin the skull under the injector. 1000nL of the G6f retro-AAV was withdrawn into the injector and lowered into layer 6 of V1. 200nL was then injected and let sit for 5 minutes. The injector was then raised to layer 4, another 200nL was injected, then raised again after 5 minutes to layer 2/3 where a third 200nL injection was made. Finally, after a 5-minute period the injector was raised to layer 1 of V1 and a final 200nL injection was made. 10 minutes after the final injection, the injector was raised out of the skull and 6-0 braided silk sutures were used to close the suture site before the mouse was taken off of anaesthesia

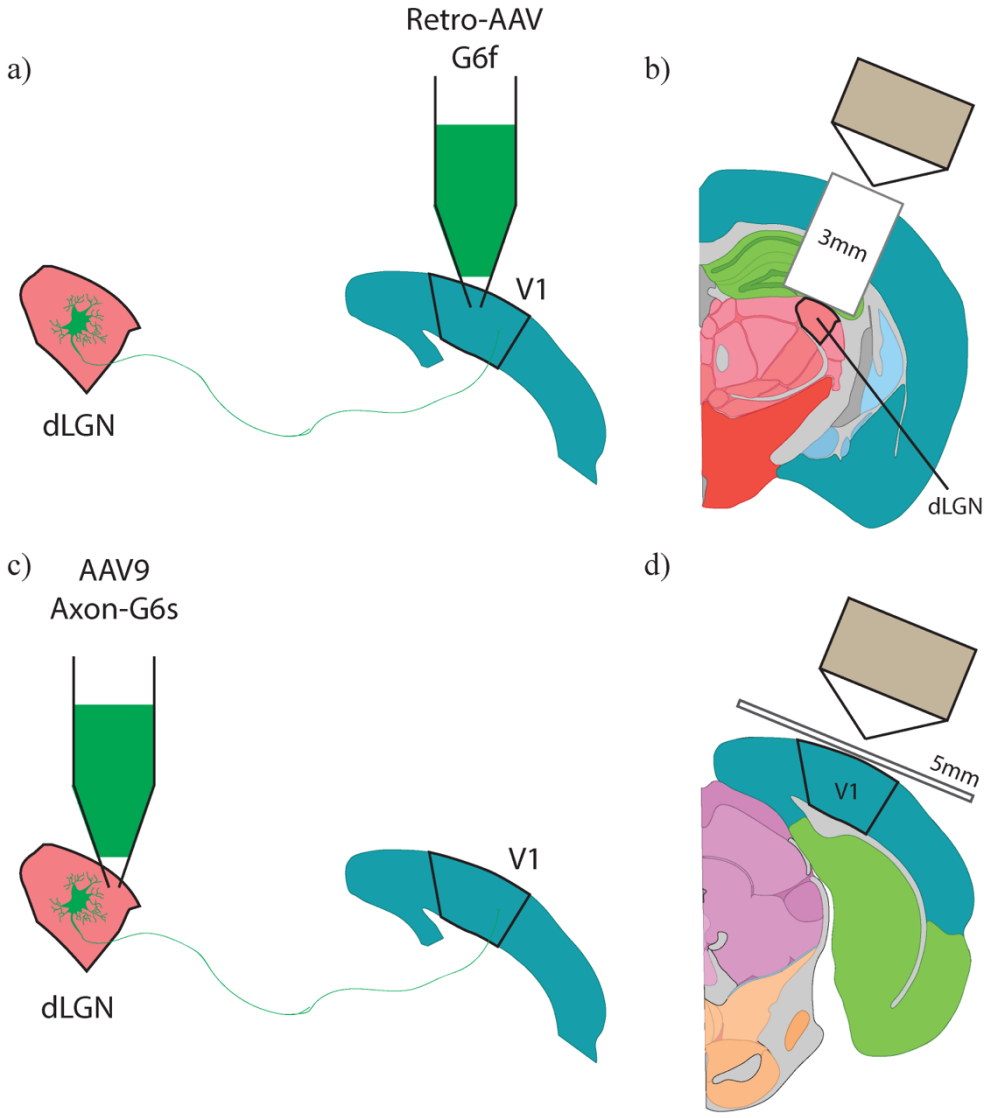


**Figure 1 | Surgical procedures provide optical access and allow for imaging LGN cells and boutons in awake behaving animals. a,** A viral injection of retrograde AAV carrying GCamP6f DNA into V1 produces calcium indicator expression in dLGN relay cell bodies in the mouse. **b,** Surgical procedure for obtaining optical access to the dLGN relay cell somas. A craniotomy above the dLGN, followed by an aspiration of the overlying brain tissue, allows for the insertion of a 3mm diameter cannula with a coverslip glued to the bottom. **c,** A viral injection of anterograde AAV9 carrying axon-GCamP6s DNA into dLGN produces calcium indicator expression in dLGN relay cell axons in the mouse. **d,** Surgical procedure for obtaining optical access to the dLGN relay cell terminals. A craniotomy above V1, followed by the placement of a 5mm diameter coverslip, provides access to relay cell terminals. Brain slice images adapted from the Allen Institute's Allen Mouse Brain Atlas[156].

and allowed to recover with a heated pad. Two weeks were given for viral uptake and expression before an implantation surgery was carried out on the injected mouse.

### 2.1.2 Cannula Implantation

To obtain optical access to the LGN cell somas, a 3mm stainless steel cannula was implanted into the skull of a mouse over the LGN (Figure 1b), a procedure adapted from Liang *et al*[4]. To create the optical cannula, a 3mm #0 thickness round cover glass was glued to the bottom of a 3mm diameter and 3mm length stainless steel tube using NOA81 fast curing optical adhesive and cured using a UV-LED.

Once the adhesive was cured, 4.8mg/kg of dexamethasone was given to the mouse intramuscularly in the caudal thigh muscle 12 hours prior to the surgical procedure. To begin the procedure, the mouse was put on anaesthesia using 5% isoflurane in balance oxygen for initiation and 0.75-2.5% isoflurane for maintenance throughout the procedure based on observed anaesthetic depth and physiological responses. Once anesthetized, the mouse was given 20mg/kg carprofen subcutaneously and 600µL of 25% mannitol in phosphate buffered saline (P.B.S) intraperitonially. Systane eye lubricant was then applied to the eyes of the mouse. Afterwards, the fur on the scalp was cleared using a trimmer and the scalp cleaned three times using 70% ethanol and 0.2% Chlorhexidine Gluconate. Once sterile, an incision 1 cm in length was made vertically across the scalp using a #15 scalpel blade, and 50µl of lidocaine/bupivacaine solution was applied to the skull. After letting the skull soak in the local anesthetic for a couple of minutes, the scalp was removed using surgical micro scissors, and any remaining connective tissue on the skull removed using micro tweezers. The tweezers were then used to separate the lateral temporalis muscle from the skull, followed by an application of Vetbond to keep the muscle separate. Surgical callipers and a surgical skin marker were then used to mark 2.7mm lateral and 1.9mm posterior to the Bregma suture and a 3 mm diameter circle was then drawn around the center point using the calipers and marker. A custom stainless steel headplate for head fixing was then positioned with

the center hole over the marked circle perpendicular to the curvature and then fixed in place using opaque C&B Metabond dental cement mixed with a small amount of activated charcoal. Once the cement was hardened, the mouse was transferred into a custom head clamp mount to keep the headplate parallel to the workbench. A dental drill with drill bit size FG ¼ was then used to begin the craniotomy and was slowly traced around the 3mm mark in the skull with periodic breaks used to cool the skull using saline. Once the skull was thinned, an EF 4 drill bit was used to drill through the skull and complete the craniotomy. After removing the skull, micro tweezers were used to perform a durotomy. A suction line attached to a 5µl unfiltered pipette tip was used to slowly aspirate the brain tissue, going through first the cortex, followed by the hippocampus, exposing the underlying LGN. Once the hippocampus was removed and the bleeding controlled, the prepared cannula was slowly inserted into the skull and positioned over the LGN. Once in place, the position was stabilised using Vetbond adhesive, and then permanently sealed using more C&B Metabond dental cement. Once the cement was hardened, the mouse was taken off anaesthesia and allowed to recover on a heating pad.

## 2.2 V1 Surgical Procedure

### 2.2.1 Viral Injections

The calcium indicator axon-GCamP6s was used to allow for LGN cell bouton imaging to measure projection responses. Expression was induced through a viral delivery using anterograde AAV9 carrying the axon-GCamP6s DNA injected into dLGN of the mouse (Figure 1c). The surgical procedure follows the same methodology as the LGN injection (outlined in § 2.1.1 Viral Injections), except the injection is performed using a single 800nL injection of virus into the LGN body (2.35mm lateral, 2.3mm posterior, 3mm ventral from the Bregma suture) followed by a 10 minute wait period before injector extraction and wound closure.

### 2.2.2 Window Implantation

To obtain optical access to the LGN cell boutons, a 5mm #0 thickness round cover glass was implanted over the visual cortex of a mouse (Figure 1d), a procedure adapted from Goldey *et al*[157].

Following the same pre-op procedure outlined in § 2.1.2 Cannula Implantation (up to and including the separation of the lateral muscle from the skull), surgical calipers were used to measure 3mm lateral and 1mm rostral to the Lambda suture, and a surgical skin marker was used to mark the point. The calipers and marker were then used to trace a 5mm diameter circle from the marked point. A custom stainless steel headplate for head fixing was then positioned with the center hole over the marked circle perpendicular to the curvature and then fixed in place using opaque C&B Metabond dental cement mixed with a small amount of activated charcoal. An FG ¼ dental drill bit was then used to thin the skull along the marked circle, with periodic saline rinses to prevent overheating of the underlying tissue. Once thinned, an EF 4 drill bit was used to drill through the skull to perform the craniotomy and the bone flap removed using micro tweezers. A 5mm #0 thickness round cover glass was then positioned over the craniotomy and affixed using LePage Super Glue Ultra Gel. A 5mm ID neodymium ring magnet was then placed centered over the cranial window. The magnet was then fixed in place and the remaining exposed skull covered using the activated charcoal opaque C&B Metabond dental cement mixture, and the mouse was allowed to recover on a heated pad.

## 2.3 Microscopy Setup

### 2.3.1 Mouse Environment

To allow for in-vivo imaging, a head fixing setup was designed using a 3D-printed running wheel and axle positioned on top of computer-controlled X-Y stage and manually controlled lab

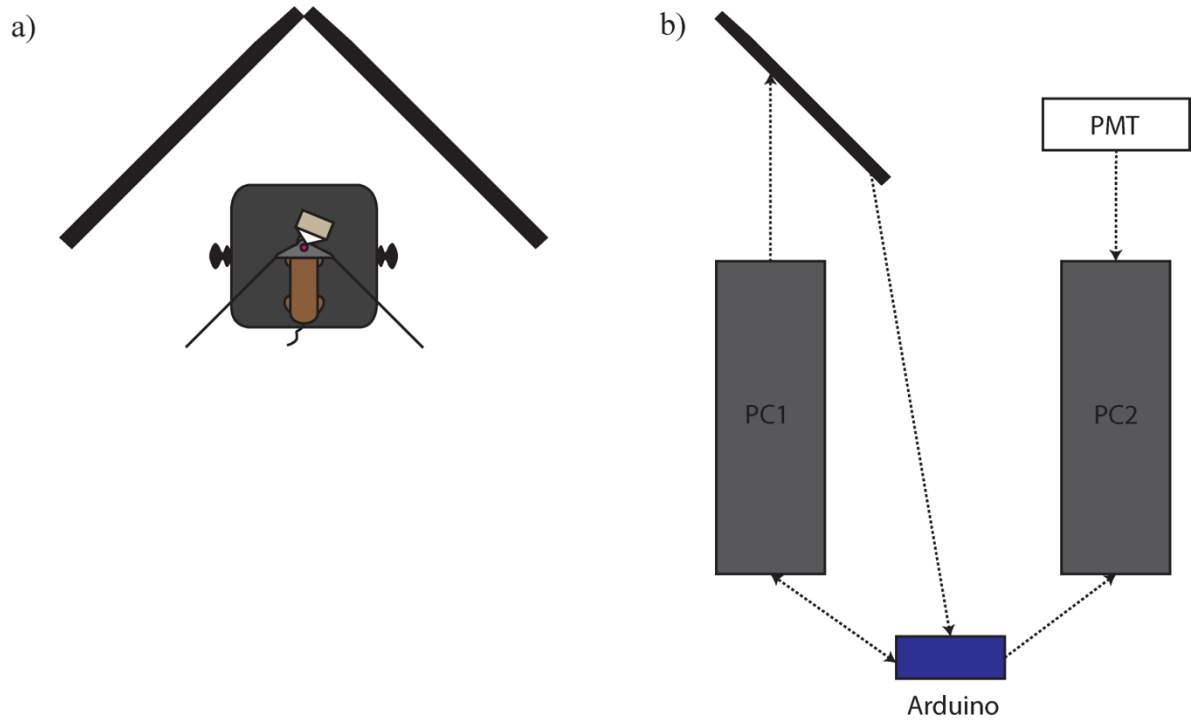


**Figure 2 | Physical setup of the behavioural environment for imaging the awake behaving mouse. a,** Setup under the microscope objective shows the mouse sitting on a running wheel positioned in front of the two monitors used for displaying visual stimuli. Head-fixing bars attach to the mounted headplate for stabilisation of the mouse head. Subfigure adapted from Wang and Krauzlis[158]. **b,** Computer setup for stimulus display and microscopy recording, showing the communication between the two computers through an Arduino intermediary. PC1 controls the stimuli presented on the screen, while PC2 records the microscopy imaging. An Arduino Uno records the refresh timing of the stimulus monitor through a photodiode, while sending out randomly timed impulse signals to both computers simultaneously for clock synchronization between the two PCs.

jack for Z positioning. Two monitors were positioned in front of the mouse for stimulus presentation. Head fixing bars, attached to posts on the X-Y stage, were positioned over the running wheel for stabilising the mouse, and the whole setup was positioned under the objective lens of the imaging microscope. A visualization of the setup is shown in Figure 2a. For the experiments performed, only the right monitor was used to isolate the stimulus for imaging the left LGN for validation of the experimental protocol, though a two-monitor setup was created for future experimental protocols.

The stimulus display monitors were controlled by a Linux machine running a Psychophysics Toolbox MATLAB script, and communicated with an Arduino Uno through a

virtual serial communications port. The microscopy imaging apparatus was controlled using a second computer running the Scanimage MATLAB program for two-photon acquisition[159] and a custom LabView script for epifluorescence acquisition. Finally, the Arduino Uno recorded monitor refresh timings using a photodiode sensor positioned over a flashing block in the corner of the stimulus monitors, and simultaneously transmitted randomly timed logic pulses to both computers for the purpose of synchronization of computer clocks to allow for the calculation of stimulus response timing. The communication setup is illustrated in Figure 2b.

### 2.3.2 Stimulus

The stimulus used for the experimental setup was a white moving bar stimulus on a dark background. The bar was created to move along its width along 8 directions on the screen, in the following order: East to West, North-West to South-East, South to North, North-East to South-West, West to East, South-East to North-West, North to South, and South-West to North-East. The width of the bar was made to be 10° in visual angle and its length was made to be the full length of the screen it was being presented on.

### 2.3.3 Calcium Imaging

To perform relay cell calcium imaging, a microscope was designed that would allow its user to perform both two-photon and epifluorescent imaging. The schematic for the custom microscope is outlined in Figure 3. The microscope objective lens was attached to a piezo stage that allowed for fast Z-axis control of the imaging plane for volume scanning, allowing for 1mm of motion along its axis. Furthermore, the two-photon microscope optics allow for simultaneous red and green fluorescence imaging as well.

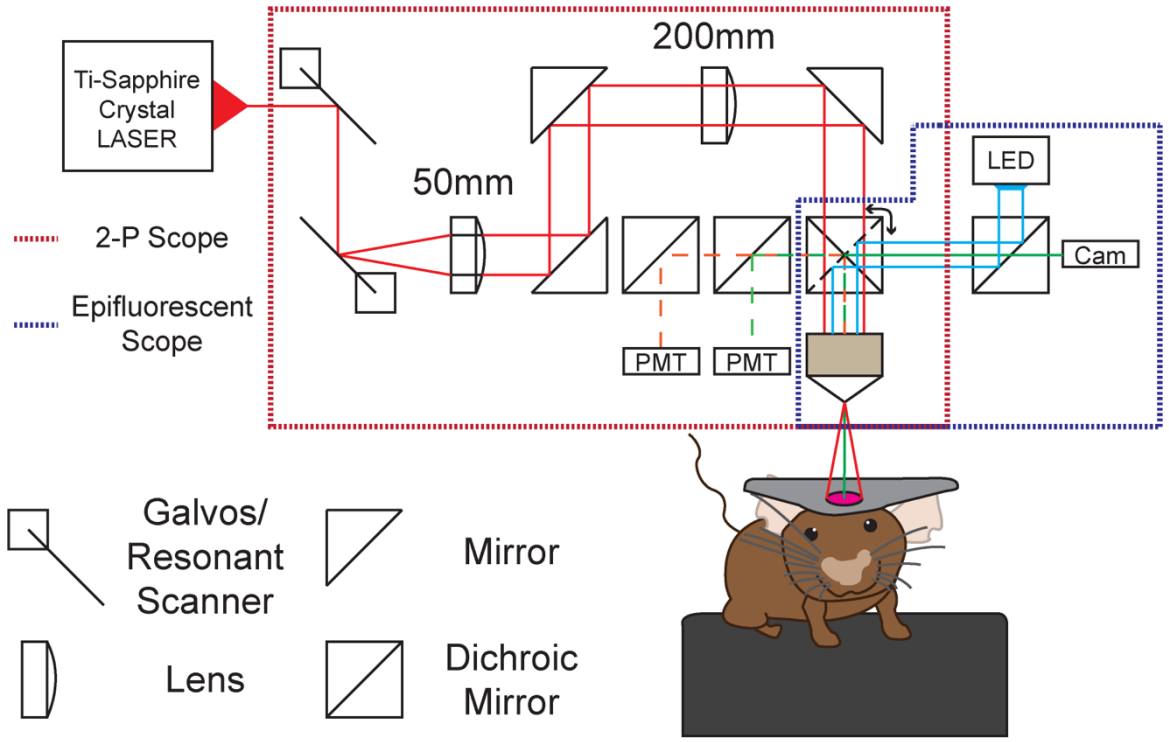


**Figure 3 | Microscope schematic showing the optical pathways for two-photon and epifluorescent imaging.** Two photon imaging utilises the Ti-Sapphire crystal laser for producing a 920-960 nm wavelength pulsed infrared laser beam for tissue excitation. The beam is scanned across the x and y axes through the rotation of a standard mirror galvanometer and resonant scanner, and the expanded beam is focused using a 50mm and 200mm lenses. The focused beam is sent through a dichroic mirror into the back of the objective lens, which stimulates the florescent neural tissue in an awake behaving mouse. Resulting fluorescence is picked up by the objective lens and reflected off the initial dichroic towards two more dichroic mirrors. The initial dichroic reflects green fluorescence to a photomultiplier tube for GCamP6 imaging, while the second dichroic reflects red fluorescence to a second photomultiplier tube to allow for simultaneous green-red fluorescence imaging. A 90° rotation of the dichroic mirror above the objective lens shifts the pathway towards the epifluorescent section. Epifluorescent imaging utilises a blue LED for broad stimulation of neural tissue, with two dichroic mirrors reflecting the blue light towards the back of the objective lens, and the resulting green fluorescence is reflected into a camera for imaging.

## 2.4 Analysis

### 2.4.1 Motion Correction

Two-photon imaging motion correction was performed using two methods to account for motion across all three axes: X, Y, and Z. To accommodate for Z motion in and out of the imaging plane, volume scanning was performed by utilising the fast-Z piezo stage attached to the objective lens. During image acquisition, the piezo stage was varied across 4 different imaging planes, each

separated by 5μm. Once the volume scans were acquired, the images were flattened into a single plane by performing an image mean during post processing.

To account for motion across the X-Y axes, a non-rigid motion correction algorithm developed for two-photon imaging, called NoRMCorre, was applied to the trial sequence[160]. By segmenting the image into equal square regions with overlapping patches, the algorithm is able to perform rigid motion correction to each individual segment and stitch each block together using the overlapping regions.

### 2.4.2 Clock Synchronization

To align the clocks of the image acquisition computer and the stimulus computer for stimulus-image analysis, randomly timed Arduino synch pulses sent to both computers simultaneously were used. Calculating the inter-pulse interval time from the pulses received by both computers and then correlating the two signals allowed for alignment of the two computer clocks to the first received pulse. A drift over time between the two clock signals post-alignment was detected and accounted for by applying a linear correlation, which proved adequate for the length of trials being performed.

### 2.4.3 Stimulus Response Analysis

Once motion correction was applied to the acquired images, regions of interest were selected and their corresponding fluorescence changes over time extracted. Ten sequential trials were averaged together to obtain their mean response property, and the signal was time correlated using the clock synchronization with the stimulus-presenting computer. A $\Delta F/F_0$ fluorescence analysis was then performed to obtain the response characteristics.

# 3 Results

## 3.1 Stimulus-Imaging Synchronization

Image acquisition and stimulus presentation timing was synchronized using the randomly timed synchronization pulses generated by the Arduino Uno and transmitted to the imaging and stimulus computer simultaneously. The raw signal pulses received by the computers and the photodiode signal received from the stimulus screen are shown in Figure 4a. By zooming in on a small subset of the sync pulses, it becomes easy to see not only the individual pulses, but also the random interval between them, along with the desynchronization between the two computers (Figure 4b). Synchronization produced accurate alignment of computer clocks, and accurately performed drift compensation over time. Taking the difference in time between subsequent pulses produces the inter-pulse interval (IPI) for the two computers (Figure 4c). The lead-lag intervals are then computed by correlating the two signals (Figure 4d), producing a strong correlation between the two (Figure 4e). Calculating the probability distribution of the IPI error between the two computers after synchronization shows that the mean error is not centered around 0 (Figure 4f). The actual IPI error itself can be seen in Figure 4g, showing the noise in the error signal, and the slight bias. To try and account for this requires calculating the correlation. The two synchronized IPI signals show strong correlation (R=1) and its slope provides information on the desynchronizing drift that occurs as a result of the non-zero error mean (Figure 4h). The transformation given by the slope calculation transforms the slowly desynchronizing signal (Figure 4i) into a stable synchronization over long periods of time (Figure 4j). This level of stability is important: Stable, synchronized stimulus-response relationships over long (~15-30min) periods of time is critical for future efforts to characterize the effects of attention, behavioral states, and genetic perturbations on the visual function of LGN neurons.

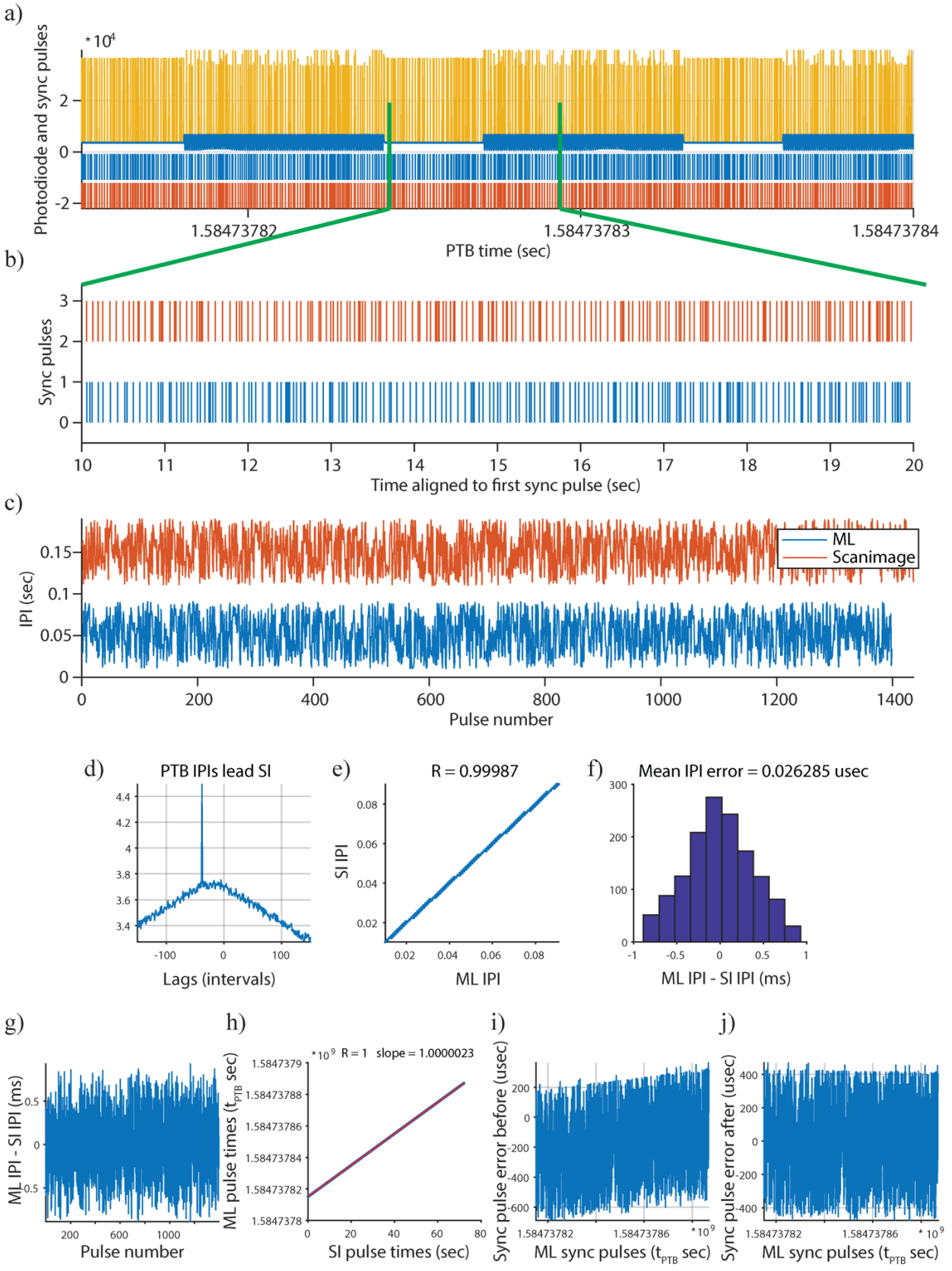
a)
Photodiode and sync pulses
*10^4
2
0
-2
1.58473782
1.58473783
1.58473784
PTB time (sec)
b)
Sync pulses
3
2
1
0
10
11
12
13
14
15
16
17
18
19
20
Time aligned to first sync pulse (sec)
c)
IPI (sec)
0.15
0.1
0.05
0
ML
Scanimage
0
200
400
600
800
1000
1200
1400
Pulse number
d)
PTB IPIs lead SI
4.4
4.2
4
3.8
3.6
3.4
-100
0
100
Lags (intervals)
e)
R = 0.99987
SI IPI
0.08
0.06
0.04
0.02
0.02
0.04
0.06
0.08
ML IPI
f)
Mean IPI error = 0.026285 usec
300
200
100
0
-1
-0.5
0
0.5
1
ML IPI - SI IPI (ms)
g)
ML IPI - SI IPI (ms)
0.5
0
-0.5
200
600
1000
Pulse number
h)
ML pulse times (t_PTB sec)
*10^9 R = 1 slope = 1.0000023
1.5847379
1.58473788
1.58473786
1.58473784
1.58473782
1.5847378
0
20
40
60
80
SI pulse times (sec)
i)
Sync pulse error before (usec)
200
0
-200
-400
-600
1.58473782
1.58473786
*10^9
ML sync pulses (t_PTB sec)
j)
Sync pulse error after (usec)
400
200
0
-200
-400
1.58473782
1.58473786
*10^9
ML sync pulses (t_PTB sec)

**Figure 4 | Randomly timed impulse signals combined with screen refresh rate monitoring allows for stimulus-imaging time synchronization and drifting clock compensation. a,** Raw signals showing the acquired sync pulses in orange and blue for the imaging (Scanimage) and stimulus (ML) computers, respectively. Raw photodiode signal from the stimulus screen is also shown. Signals are plotted relative to the computer clock of the stimulus computer as obtained through psychophysics toolbox (PTB). **b,** A time-zoomed portion of the first graph with individual sync pulses of both computers visible. A misalignment of the obtained pulses is evident. **c,** Graph of the inter-pulse interval (IPI) of the signals of both computers, showing the time difference between subsequent pulses. **d,** Correlation strength of different lag periods, showing a strong correlation of the signals when a proper time lag is applied to align the pulses obtained in the two computers. **e,** Correlation plot of the time aligned IPIs showing strong correlation (R=0.99987). **f,** Plot of the distribution of the IPI error between the two computers. The non-zero distribution mean is noted, implicating the existence of a drift between the clocks of the two computers. **g,** plot of the IPI error between the two computers for each pulse. **h,** Pulse times plotted against each other for both computers. A strong correlation (R=1) implies a stable desynchronizing drift, while the slope (m=1.0000023) characterizes the desynchronizing drift. **i,** Plot of the sync pulse error before a correction is applied, showing an evident slow drift over time. **j,** Sync pulse error after a correction for time-drift is applied, showing a zero-mean stabilization of the sync pulse error.

## 3.2 LGN Imaging

The GCamP6f-expressing LGN of an awake behaving mouse being presented moving bar stimuli was imaged using both epifluorescent microscopy (Figure 5a) and 2p microscopy (Figure 5b). Based on these maps, we were able to then center the microscope's field of view on a responsive location and switch to two-photon imaging. Once the two-photon response videos were obtained, motion compensation was applied to the 2p image and time synchronization allowed for stimulus response analysis. Fluorescence changes of two different regions of interest were compared for differences in response properties and were plotted versus stimulus display time (Figure 5c). To get a better sense of the responses seen within the whole imaged region, 50 cell regions were further compared using a pixel-intensity image plot to look at alignment of response timings of a large number of cells in the imaged region (Figure 5d). Responses were easily distinguishable from background noise, and in a few example cells, showed preferential responses to the direction of the moving bar.

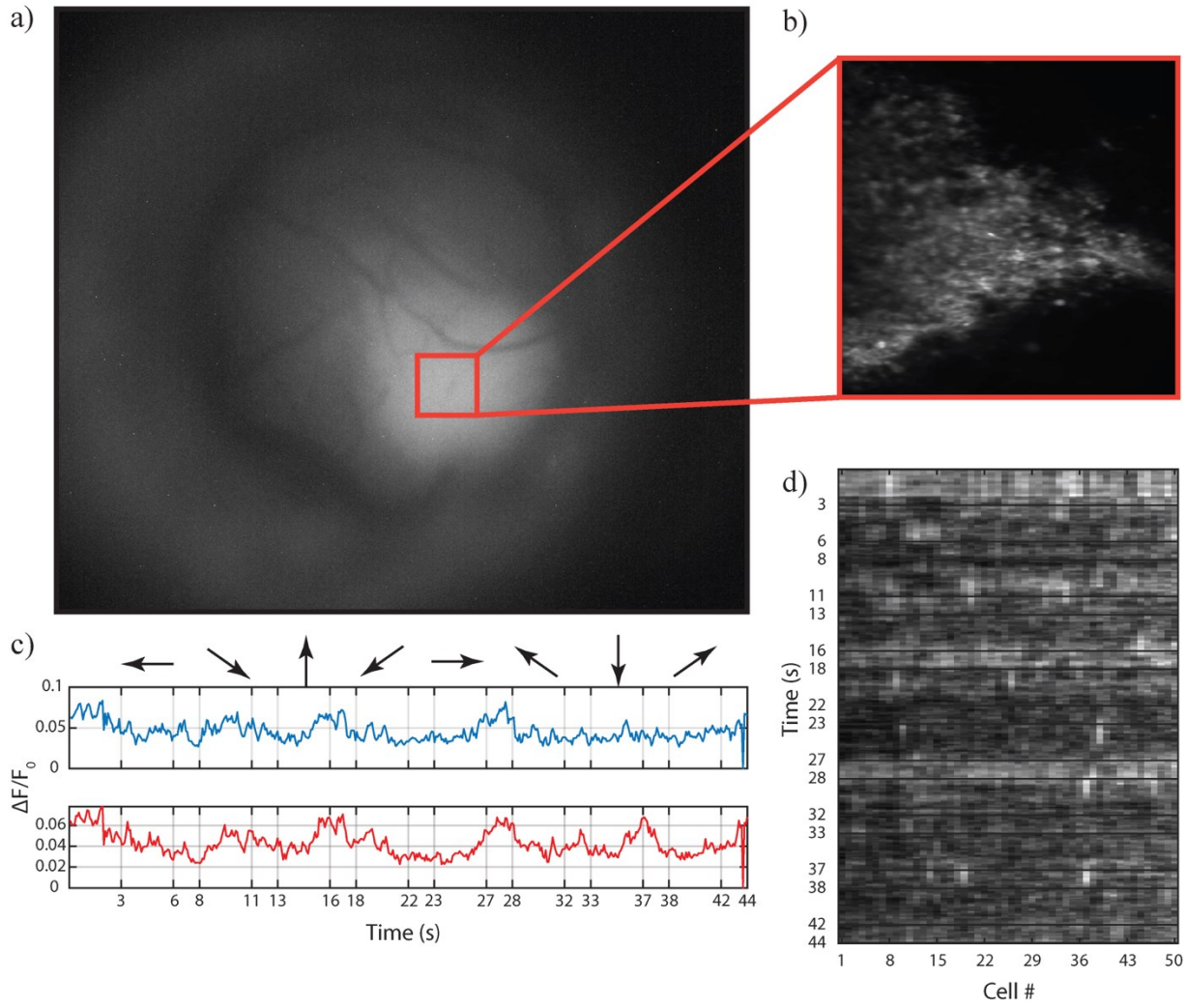


**Figure 5 | In vivo imaging of LGN relay cells. a,** An epifluorescent image obtained through a cannula implanted into a mouse. Blood vessels are visible on the surface of the exposed brain region, as well as the fluorescing LGN. **b,** Image of fluorescing LGN cell bodies obtained using 2p microscopy on an awake behaving mouse. **c,** $\Delta F/F_0$ of two sample cells within the imaged region. Stimulus timing with corresponding bar directions are shown. Intermediary regions are grey screens with no moving bar present. **d,** Visual plot of 50 different regions of interest, showing visible response patterns in all of the sampled cells.

## 3.3 V1 Imaging

Next, we imaged axon-GCamP6s expressing LGN terminals in V1 during moving bar stimulus displays. Epifluorescent imaging of V1 (Figure 6a) allowed for retinotopic mapping of the cortical projections as compared to visual space represented by the stimulus displaying screen. A sample point in V1 was analysed for the moving bar stimuli to determine its retinotopic

coordinates on the screen for four bar directions (dorsal, ventral, nasal, and temporal). The bar centroids representing the location during the strongest fluorescence response were plotted on a representative stimulus screen (Figure 6b). By applying the same principle to each pixel in the epifluorescent image, retinotopic heat maps were developed showing the frame that elicited the strongest fluorescence response for each bar direction, with colours representing the different timing. Figure 6c shows a sample heat map for an East to West moving bar. Afterwards, layer 1 of V1 LGN terminals were imaged using 2p microscopy (Figure 6d). After motion correction was applied, a fluorescence analysis of 20 boutons was plotted showing varying responses across the different LGN boutons (Figure 6e). Finally, the boutons were then analysed for direction or orientation preferences, with three representative bouton types shown in Figure 6f.

# 4 Discussion

## 4.1 Synchronization

The results of the timing analysis show that clock synchronization between the two computers is feasible and can account for clock desynchronization that occurs through a linear relation. Computational clock-keeping utilises a quartz crystal oscillator, and various phenomena can affect the stability and noise in the oscillator. The sources of instability, such as ionizing radiation and temperature, are likely responsible for the noise in the inter-pulse interval error, and coupled with minor variations in base crystal frequency would result in a time drift as well (for a more detailed discussion on crystal oscillator stability, refer to *Walls & Vig*[161]).

## 4.2 LGN Imaging

LGN imaging results show that cannula implantations could serve as a useful method for assessing geniculate cell responses and introduces a host of potential experiments using the method to better understand feature processing and representation across the LGN itself. The method could

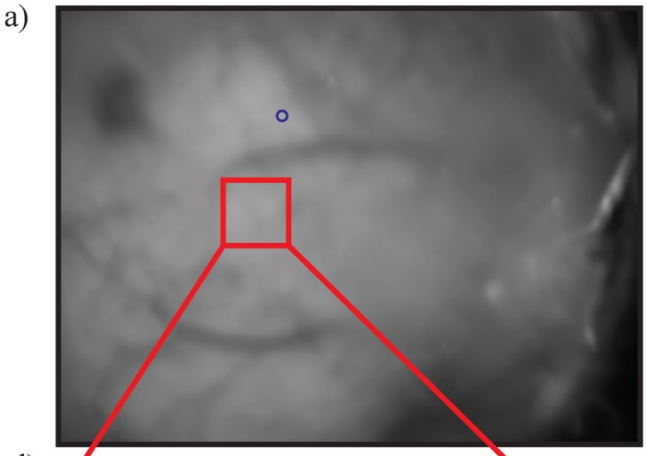
a)

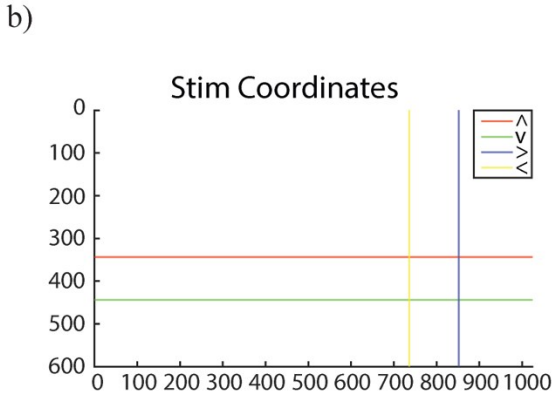
b)
Stim Coordinates
^
v
>
<
0
100
200
300
400
500
600
0 100 200 300 400 500 600 700 800 900 1000

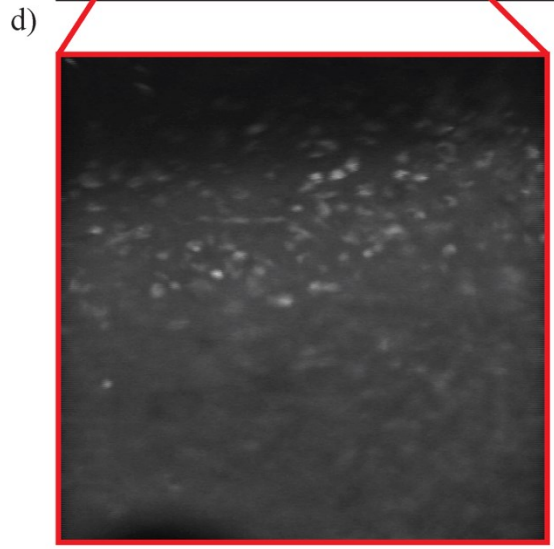
d)

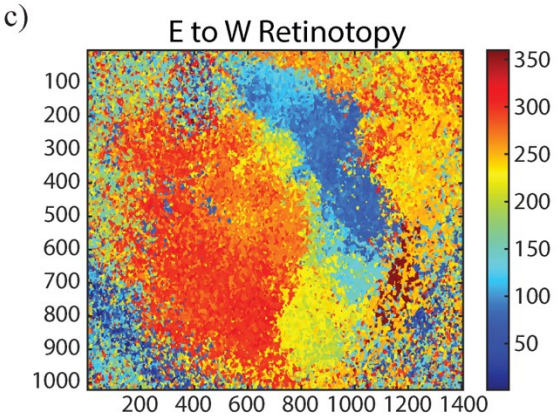
c)
E to W Retinotopy
100
200
300
400
500
600
700
800
900
1000
200 400 600 800 1000 1200 1400
350
300
250
200
150
100
50

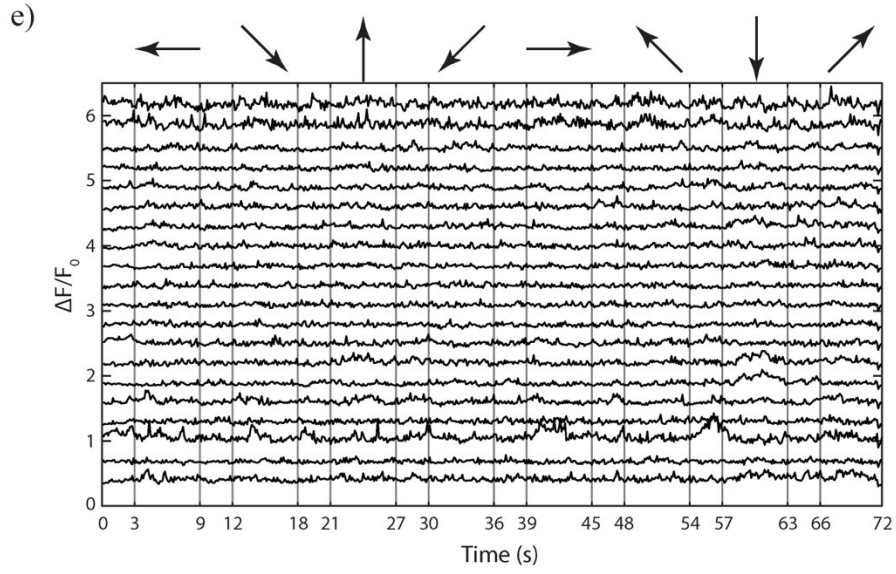
e)
ΔF/F0
0
1
2
3
4
5
6
0 3 9 12 18 21 27 30 36 39 45 48 54 57 63 66 72
Time (s)

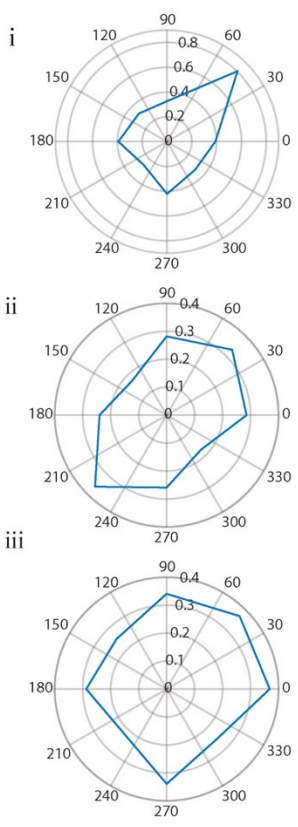
f)
i
ii
iii
90
120
60
150
30
180
0
210
330
240
300
270
0.8
0.6
0.4
0.2
0.3
0.1

**Figure 6 | In vivo imaging of LGN relay terminals in V1. a,** An epifluorescent image obtained through a cortical window implanted into a mouse. Blood vessels are visible on the surface of the exposed brain region, as well as the fluorescing LGN terminals in V1. **b,** Retinotopic coordinates of the sampled blue point in the epifluorescent image. Each colour represents one of four moving bars, and the coordinates represents the center of the bar on the stimulus screen when the strongest response was elicited in the sampled point. Intersection of the bars represents the receptive field location of the sample region relative to the screen. **c,** The retinotopic map of the imaged region for a bar moving east to west. Heat map represents the frame time when the strongest response was elicited in that region. **d,** 2p image of LGN terminals in V1 layer 1 of an awake mouse. **e,** Normalized fluorescence changes of 20 axon terminal regions. Stimulus timings and the respective direction of the moving bar are shown. **f,** Three sample boutons representative of the response types seen in the 20 imaged terminals, with responses plotted on a polar plot. Plotted angle represents the direction of bar movement on the screen, and radius the relative strength of the response. Sample terminals with directional tuning (*i),* with orientation tuning (*ii),* and with no obvious directional or orientational preference (*iii).*

be used to understand whether the non-uniform feature mapping seen by *Piscopo et al.*[3] is a result of local processing within the geniculate or whether it is a result of variations in retinal input strength. By comparing the response properties of individual relay cell neurons based on retinotopic location, the non-uniformity can be mapped. Similarly, through the use of GAD-67 Cre lines[128] and Cre-dependant GCamP6f injections into the LGN, inhibitory interneuron responses could be imaged and their outputs compared to the feature mapping of the relay cells. Intensity-based glutamate-sensing fluorescent reporters (iGluSnFRs) allow for optical imaging of glutamate release[162] and would allow for the detection of increased signaling strength of RGCs in enriched versus depleted feature zones in the LGN, presenting an opportunity to understand the contrast between inhibition in depleted areas and increased excitation in enriched areas.

The role of inhibition in feature representations across the LGN could then be further explored through the use of trans-synaptic tracing using Cre and Flp AAVs[163]. By utilising a GAD-67 Cre mouseline, injecting a Cre-dependant Flp virus into different LGN projecting brain regions, such as the superior colliculus or thalamic reticular nucleus, and a Flp-dependant GCamP6f into the LGN itself, it would be possible to image the responses of inhibitory cells receiving projections from specific brain regions. If the non-uniform feature mapping is a result of local inhibition, such

an experiment would allow for an understanding of how different LGN-projecting regions contribute to this non-uniformity.

A similar experimental protocol could be combined with DREADDs or optogenetics to force expression of these receptors on specific inhibitory interneurons in the LGN and perturbations of these cells combined with GCamP6f imaging of the thalamocortical relay cells would give the experimenter an opportunity to understand how variations in signaling of these cells could affect the feature representation in the LGN.

The implementation of a lick spout into the microscopy environment would allow for visually-driven behavioural assessments[158]. Utilising this behavioural setup would allow for an assessment of the behavioural relevance of these non-uniform feature representations by presenting the specific feature stimuli in different parts of the visual field and analyzing the stimuli-detection performance of the mouse. Then, the use of DREADDs or optogenetics could be used to assess the behavioural impact of perturbations in the specific LGN circuits.

Furthermore, it was found that the corticothalamic feedback projections from V1 are necessary for RGC synapse formation in the LGN as determined through the use of Tra2β mutant mice[164]. By utilising these mice and the cannula imaging protocol, it would be possible to decouple the RGC and V1 inputs to the LGN and image the response properties of the LGN cells to gain a better understanding of the role of other geniculate-projecting brain regions. These mice would also simplify the surgical protocol by removing the need for a cortical aspiration, reducing the potential for tissue damage as a result of bleeding or trauma to the LGN.

Finally, adapting the developed surgical protocol to utilise two-photon miniscopes in free-moving mice[165] would allow the experimenter to image LGN signal responses during ethologically relevant visual behaviours such as cricket hunting[166]. Utilising the discussed perturbation methods

would also provide a greater understanding of the behavioural relevance of these circuits in free-moving mice.

## 4.3 V1 Imaging

The results of the V1 imaging protocol test shows that it is possible to image layer-specific LGN bouton terminals to obtain their response properties. Imaging LGN terminals in this fashion would allow for a more in-depth understanding of how lamination patterns of the LGN projections are related to LGN cell feature mapping. Furthermore, given that the LGN cannula protocol resorts to cortical aspiration to obtain optical access, it is possible that the response properties would be affected due to a change in corticothalamic feedback. By imaging LGN terminals in V1, all feedback projections are maintained, allowing for a more robust mapping of LGN feature space. Given that both the cell bodies and the projections follow a specific retinotopy, it would be possible to infer the cell body location based on the retinotopic location of the terminals themselves. The experiments would therefore provide an opportunity to perform a comparison study to understand the importance of maintaining the corticothalamic feedback projections on the LGN cell body response properties. Furthermore, V1 imaging would also provide an understanding of any potential non-uniformity of feature distribution in LGN cell projections across the different cortical layers.

Given the potential for axo-axonal inhibition of LGN relay terminals by cortical interneurons, it would be possible to utilise the DREADD and optogenetic approaches to perturb cortical interneurons and see whether they affect the feature response properties of the LGN relay cell terminals in V1. The experiment would provide information on not only the way the feature distribution is imparted in V1, but also on the way cortical interneurons might further enhance certain feature representations in various parts of visual space. Visually driven behavioural tasks

would also provide information on the importance of these cortical circuits on behavioural performance.

Utilising red calcium indicators, such as the jRGECO1a protein[167], would allow for simultaneous imaging of LGN relay cells and V1 cortical cells simultaneously. By injecting anterograde axon-GCamP6s into LGN and anterograde jRGECO1a into V1, the different signals would be differentiable based on the fluorescence colour, a capacity that the custom two-photon microscope was developed with.

Finally, the V1 cranial window imaging protocol could be combined with the trans-synaptic tracing method to image LGN relay cells that obtain specific RGC inputs. By using a Cre-dependant Flp injected into the eye, a Flp-dependant axon-GCamP6s injected into LGN, and a Cre driver line isolated for specific RGC cell types, it would be possible to image the relay cell bouton feature response properties based on the specific type of RGC input they obtain.

# 5 Conclusion

Understanding how the LGN receives, transforms, and transmits the retinal signal is an important step towards understanding how conscious vision arises, and how it drives visual behaviour. While the non-uniformity of feature representations in the LGN has been reported on, the exact neural circuits that allow this to happen are not understood. Two surgical protocols, a microscopy setup, and an image processing pipeline were developed and the preliminary results indicate the capacity to image both geniculate cells and boutons, laying the groundwork for future experiments that would allow for gaining a deeper appreciation of the neural system in the LGN and its important role in visual processing.

# 6 References

1. Masland, R. H. The fundamental plan of the retina. *Nat. Neurosci.* **4**, 877–886 (2001).

2. Seabrook, T. A., Burbridge, T. J., Crair, M. C. & Huberman, A. D. Architecture, Function, and Assembly of the Mouse Visual System. *Annu. Rev. Neurosci.* **40**, 499–538 (2017).

3. Piscopo, D. M., El-Danaf, R. N., Huberman, A. D. & Niell, C. M. Diverse Visual Features Encoded in Mouse Lateral Geniculate Nucleus. *J. Neurosci.* **33**, 4642–4656 (2013).

4. Liang, L. *et al.* A Fine-Scale Functional Logic to Convergence from Retina to Thalamus. *Cell* **173**, 1343-1355.e24 (2018).

5. Morgan, J. L., Berger, D. R., Wetzel, A. W. & Lichtman, J. W. The Fuzzy Logic of Network Connectivity in Mouse Visual Thalamus. *Cell* **165**, 192–206 (2016).

6. Masland, R. H. The Neuronal Organization of the Retina. *Neuron* **76**, 266–280 (2012).

7. Lagnado, L. & Baylor, D. Signal flow in visual transduction. *Neuron* **8**, 995–1002 (1992).

8. Rieke, F. & Baylor, D. A. Single-photon detection by rod cells of the retina. *Rev. Mod. Phys.* **70**, 1027–1036 (1998).

9. Lolley, R. N. & Lee, R. H. Cyclic GMP and photoreceptor function. *FASEB J.* **4**, 3001–3008 (1990).

10. Carroll, J., Neitz, M., Hofer, H., Neitz, J. & Williams, D. R. Functional photoreceptor loss revealed with adaptive optics: An alternate cause of color blindness. *Proc. Natl. Acad. Sci.* **101**, 8461–8466 (2004).

11. Deeb, S. S. The molecular basis of variation in human color vision. *Clin. Genet.* **67**, 369–377 (2005).

12. Striessnig, J., Pinggera, A., Kaur, G., Bock, G. & Tuluc, P. L-type Ca2+ channels in heart and brain. *Wiley Interdiscip. Rev. Membr. Transp. Signal.* **3**, 15–38 (2014).

13. Matthews, G. & Fuchs, P. The diverse roles of ribbon synapses in sensory neurotransmission. *Nat. Rev. Neurosci.* **11**, 812–822 (2010).

14. Lasater, E. M. Retinal horizontal cell gap junctional conductance is modulated by dopamine through a cyclic AMP-dependent protein kinase. *Proc. Natl. Acad. Sci.* **84**, 7319–7323 (1987).

15. Mangel, S. C. Analysis of the horizontal cell contribution to the receptive field surround of ganglion cells in the rabbit retina. *J. Physiol.* **442**, 211–234 (1991).

16. Kirsch, M., Wagner, H.-J. & Djamgoz, M. B. A. Dopamine and plasticity of horizontal cell function in the teleost retina: Regulation of a spectral mechanism through D1-receptors. *Vision Res.* **31**, 401–412 (1991).

17. Hampson, E. C. G. M., Weiler, R. & Vaney, D. I. pH-gated dopaminergic modulation of horizontal cell gap junctions in mammalian retina. *Proc. R. Soc. Lond. B Biol. Sci.* **255**, 67–72 (1994).

18. Barnes, S. & Kelly, M. E. M. Calcium Channels at the Photoreceptor Synapse. in *Photoreceptors and Calcium* (eds. Baehr, W. & Palczewski, K.) 465–476 (Springer US, 2002). doi:10.1007/978-1-4615-0121-3_28.

19. Herrmann, R. *et al.* Rod Vision Is Controlled by Dopamine-Dependent Sensitization of Rod Bipolar Cells by GABA. *Neuron* **72**, 101–110 (2011).

20. Kemmler, R., Schultz, K., Dedek, K., Euler, T. & Schubert, T. Differential Regulation of Cone Calcium Signals by Different Horizontal Cell Feedback Mechanisms in the Mouse Retina. *J. Neurosci.* **34**, 11826–11843 (2014).

21. Wässle, H., Puller, C., Müller, F. & Haverkamp, S. Cone contacts, mosaics, and territories of bipolar cells in the mouse retina. *J. Neurosci. Off. J. Soc. Neurosci.* **29**, 106–117 (2009).

22. Euler, T. & Masland, R. H. Light-Evoked Responses of Bipolar Cells in a Mammalian Retina. *J. Neurophysiol.* **83**, 1817–1829 (2000).

23. DeVries, S. H. Bipolar Cells Use Kainate and AMPA Receptors to Filter Visual Information into Separate Channels. *Neuron* **28**, 847–856 (2000).

24. Shen, Y. *et al.* A Transient Receptor Potential-Like Channel Mediates Synaptic Transmission in Rod Bipolar Cells. *J. Neurosci.* **29**, 6088–6093 (2009).

25. Koike, C. *et al.* TRPM1 is a component of the retinal ON bipolar cell transduction channel in the mGluR6 cascade. *Proc. Natl. Acad. Sci.* **107**, 332–337 (2010).

26. Bloomfield, S. A. & Dacheux, R. F. Rod Vision: Pathways and Processing in the Mammalian Retina. *Prog. Retin. Eye Res.* **20**, 351–384 (2001).

27. Wässle, H. Parallel processing in the mammalian retina. *Nat. Rev. Neurosci.* **5**, 747–757 (2004).

28. Hoshi, H., Liu, W.-L., Massey, S. C. & Mills, S. L. ON Inputs to the OFF Layer: Bipolar Cells That Break the Stratification Rules of the Retina. *J. Neurosci.* **29**, 8875–8883 (2009).

29. Dumitrescu, O. N., Pucci, F. G., Wong, K. Y. & Berson, D. M. Ectopic retinal ON bipolar cell synapses in the OFF inner plexiform layer: Contacts with dopaminergic amacrine cells and melanopsin ganglion cells. *J. Comp. Neurol.* **517**, 226–244 (2009).

30. Famiglietti, E. V. Synaptic organization of starburst amacrine cells in rabbit retina: Analysis of serial thin sections by electron microscopy and graphic reconstruction. *J. Comp. Neurol.* **309**, 40–70 (1991).

31. Vaney, D. I. & Pow, D. V. The dendritic architecture of the cholinergic plexus in the rabbit retina: Selective labeling by glycine accumulation in the presence of sarcosine. *J. Comp. Neurol.* **421**, 1–13 (2000).

32. Huberman, A. D. *et al.* Genetic Identification of an On-Off Direction- Selective Retinal Ganglion Cell Subtype Reveals a Layer-Specific Subcortical Map of Posterior Motion. *Neuron* **62**, 327–334 (2009).

33. MacNeil, M. A. & Masland, R. H. Extreme Diversity among Amacrine Cells: Implications for Function. *Neuron* **20**, 971–982 (1998).

34. Masland, R. H. The tasks of amacrine cells. *Vis. Neurosci.* **29**, 3–9 (2012).

35. Ackman, J. B., Burbridge, T. J. & Crair, M. C. Retinal waves coordinate patterned activity throughout the developing visual system. *Nature* **490**, 219–225 (2012).

36. Grimes, W. N., Zhang, J., Graydon, C. W., Kachar, B. & Diamond, J. S. Retinal Parallel Processors: More than 100 Independent Microcircuits Operate within a Single Interneuron. *Neuron* **65**, 873–885 (2010).

37. Demb, J. B. Cellular Mechanisms for Direction Selectivity in the Retina. *Neuron* **55**, 179–186 (2007).

38. Hirasawa, H., Contini, M. & Raviola, E. Extrasynaptic release of GABA and dopamine by retinal dopaminergic neurons. *Philos. Trans. R. Soc. B Biol. Sci.* **370**, (2015).

39. Rheaume, B. A. *et al.* Single cell transcriptome profiling of retinal ganglion cells identifies cellular subtypes. *Nat. Commun.* **9**, 2759 (2018).

40. Mastronarde, D. N. Two types of cat retinal ganglion cells that are suppressed by contrast. *Vision Res.* **25**, 1195–1196 (1985).

41. Krishnaswamy, A., Yamagata, M., Duan, X., Hong, Y. K. & Sanes, J. R. Sidekick 2 directs formation of a retinal circuit that detects differential motion. *Nature* **524**, 466–470 (2015).

42. Mason, C. A. & Sretavan, D. W. Glia, neurons, and axon pathfinding during optic chiasm development. *Curr. Opin. Neurobiol.* **7**, 647–653 (1997).

43. Neveu, M. M. & Jeffery, G. Chiasm formation in man is fundamentally different from that in the mouse. *Eye* **21**, 1264–1270 (2007).

44. Stone, J., Leicester, J. & Sherman, S. M. The naso-temporal division of the monkey's retina. *J. Comp. Neurol.* **150**, 333–348 (1973).

45. Dräger, U. C. & Olsen, J. F. Origins of crossed and uncrossed retinal projections in pigmented and albino mice. *J. Comp. Neurol.* **191**, 383–412 (1980).

46. Morin, L. P. & Studholme, K. M. Retinofugal projections in the mouse. *J. Comp. Neurol.* **522**, 3733–3753 (2014).

47. Monavarfeshani, A., Sabbagh, U. & Fox, M. A. Not a one-trick pony: Diverse connectivity and functions of the rodent lateral geniculate complex. *Vis. Neurosci.* **34**, (2017).

48. Rodieck, R. W., Binmoeller, K. F. & Dineen, J. Parasol and midget ganglion cells of the human retina. *J. Comp. Neurol.* **233**, 115–132 (1985).

49. Leventhal, A. G., Rodieck, R. W. & Dreher, B. Retinal ganglion cell classes in the Old World monkey: morphology and central projections. *Science* **213**, 1139–1142 (1981).

50. Hendry, S. H. & Yoshioka, T. A neurochemically distinct third channel in the macaque dorsal lateral geniculate nucleus. *Science* **264**, 575–577 (1994).

51. Shapley, R. & Perry, V. H. Cat and monkey retinal ganglion cells and their visual functional roles. *Trends Neurosci.* **9**, 229–235 (1986).

52. Merigan, W. H., Byrne, C. E. & Maunsell, J. H. Does primate motion perception depend on the magnocellular pathway? *J. Neurosci.* **11**, 3422–3429 (1991).

53. Irvin, G. E., Casagrande, V. A. & Norton, T. T. Center/surround relationships of magnocellular, parvocellular, and koniocellular relay cells in primate lateral geniculate nucleus. *Vis. Neurosci.* **10**, 363–373 (1993).

54. Klistorner, A., Crewther, D. P. & Crewther, S. G. Separate magnocellular and parvocellular contributions from temporal analysis of the multifocal VEP. *Vision Res.* **37**, 2161–2169 (1997).

55. McMahon, M. J., Lankheet, M. J. M., Lennie, P. & Williams, D. R. Fine Structure of Parvocellular Receptive Fields in the Primate Fovea Revealed by Laser Interferometry. *J. Neurosci.* **20**, 2043–2053 (2000).

56. Solomon, S. G., White, A. J. R. & Martin, P. R. Extraclassical Receptive Field Properties of Parvocellular, Magnocellular, and Koniocellular Cells in the Primate Lateral Geniculate Nucleus. *J. Neurosci.* **22**, 338–349 (2002).

57. Shapley, R. Parallel Retinocortical Channels: X and Y and P and M. in *Advances in Psychology* (ed. Brannan, J. R.) vol. 86 3–36 (North-Holland, 1992).

58. Hendry, S. H. & Reid, R. C. The koniocellular pathway in primate vision. *Annu. Rev. Neurosci.* **23**, 127–153 (2000).

59. Sincich, L. C., Park, K. F., Wohlgemuth, M. J. & Horton, J. C. Bypassing V1: a direct geniculate input to area MT. *Nat. Neurosci.* **7**, 1123–1128 (2004).

60. Horn, S. C. V., Erişir, A. & Sherman, S. M. Relative distribution of synapses in the A-laminae of the lateral geniculate nucleus of the cat. *J. Comp. Neurol.* **416**, 509–520 (2000).

61. Munoz, D. P. & Wurtz, R. H. Role of the rostral superior colliculus in active visual fixation and execution of express saccades. *J. Neurophysiol.* **67**, 1000–1002 (1992).

62. Munoz, D. P. & Wurtz, R. H. Saccade-related activity in monkey superior colliculus. I. Characteristics of burst and buildup cells. *J. Neurophysiol.* **73**, 2313–2333 (1995).

63. Hafed, Z. M., Goffart, L. & Krauzlis, R. J. A Neural Mechanism for Microsaccade Generation in the Primate Superior Colliculus. *Science* **323**, 940–943 (2009).

64. Lyon, D. C., Nassi, J. J. & Callaway, E. M. A Disynaptic Relay from Superior Colliculus to Dorsal Stream Visual Cortex in Macaque Monkey. *Neuron* **65**, 270–279 (2010).

65. Kinoshita, M. *et al.* Dissecting the circuit for blindsight to reveal the critical role of pulvinar and superior colliculus. *Nat. Commun.* **10**, 135 (2019).

66. Bickford, M. E., Zhou, N., Krahe, T. E., Govindaiah, G. & Guido, W. Retinal and Tectal "Driver-Like" Inputs Converge in the Shell of the Mouse Dorsal Lateral Geniculate Nucleus. *J. Neurosci.* **35**, 10523–10534 (2015).

67. Ahmadlou, M., Zweifel, L. S. & Heimel, J. A. Functional modulation of primary visual cortex by the superior colliculus in the mouse. *Nat. Commun.* **9**, 3895 (2018).

68. Shannon, C. E. A mathematical theory of communication. *Bell Syst. Tech. J.* **27**, 379–423 (1948).

69. Eckhorn, R. & Pöpel, B. Rigorous and extended application of information theory to the afferent visual system of the cat. I. Basic concepts. *Kybernetik* **16**, 191–200 (1974).

70. Eckhorn, R. & Pöpel, B. Rigorous and extended application of information theory to the afferent visual system of the cat. II. Experimental results. *Biol. Cybern.* **17**, 7–17 (1975).

71. Hicks, T. P., Lee, B. B. & Vidyasagar, T. R. The responses of cells in macaque lateral geniculate nucleus to sinusoidal gratings. *J. Physiol.* **337**, 183–200 (1983).

72. White, A. J. R., Solomon, S. G. & Martin, P. R. Spatial properties of koniocellular cells in the lateral geniculate nucleus of the marmoset Callithrix jacchus. *J. Physiol.* **533**, 519–535 (2001).

73. Singer, W. & Bedworth, N. Inhibitory interaction between X and Y units in the cat lateral geniculate nucleus. *Brain Res.* **49**, 291–307 (1973).

74. Van Hooser, S. D., Heimel, J. A. F. & Nelson, S. B. Receptive Field Properties and Laminar Organization of Lateral Geniculate Nucleus in the Gray Squirrel (Sciurus carolinensis). *J. Neurophysiol.* **90**, 3398–3418 (2003).

75. Luo, L., Callaway, E. M. & Svoboda, K. Genetic Dissection of Neural Circuits. *Neuron* **57**, 634–660 (2008).

76. Nagel, G. *et al.* Channelrhodopsin-2, a directly light-gated cation-selective membrane channel. *Proc. Natl. Acad. Sci.* **100**, 13940–13945 (2003).

77. Roth, B. L. DREADDs for Neuroscientists. *Neuron* **89**, 683–694 (2016).

78. Chen, T.-W. *et al.* Ultra-sensitive fluorescent proteins for imaging neuronal activity. *Nature* **499**, 295–300 (2013).

79. Beck, C. & Gong, Y. A high-speed, bright, red fluorescent voltage sensor to detect neural activity. *Sci. Rep.* **9**, 15878 (2019).

80. Fenno, L., Yizhar, O. & Deisseroth, K. The Development and Application of Optogenetics. *Annu. Rev. Neurosci.* **34**, 389–412 (2011).

81. Yizhar, O., Fenno, L. E., Davidson, T. J., Mogri, M. & Deisseroth, K. Optogenetics in Neural Systems. *Neuron* **71**, 9–34 (2011).

82. Leinweber, M. *et al.* Two-photon Calcium Imaging in Mice Navigating a Virtual Reality Environment. *J. Vis. Exp. JoVE* (2014) doi:10.3791/50885.

83. Poort, J. *et al.* Learning Enhances Sensory and Multiple Non-sensory Representations in Primary Visual Cortex. *Neuron* **86**, 1478–1490 (2015).

84. Calderone, J. B. & Jacobs, G. H. Regional variations in the relative sensitivity to UV light in the mouse retina. *Vis. Neurosci.* **12**, 463–468 (1995).

85. Joesch, M. & Meister, M. A neuronal circuit for colour vision based on rod–cone opponency. *Nature* **532**, 236–239 (2016).

86. Jeon, C.-J., Strettoi, E. & Masland, R. H. The Major Cell Populations of the Mouse Retina. *J. Neurosci.* **18**, 8936–8946 (1998).

87. Curcio, C. A., Sloan, K. R., Kalina, R. E. & Hendrickson, A. E. Human photoreceptor topography. *J. Comp. Neurol.* **292**, 497–523 (1990).

88. Krahe, T. E., El-Danaf, R. N., Dilger, E. K., Henderson, S. C. & Guido, W. Morphologically Distinct Classes of Relay Cells Exhibit Regional Preferences in the Dorsal Lateral Geniculate Nucleus of the Mouse. *J. Neurosci.* **31**, 17437–17448 (2011).

89. Baden, T. *et al.* The functional diversity of retinal ganglion cells in the mouse. *Nature* **529**, 345–350 (2016).

90. Famiglietti, E. V. & Kolb, H. Structural basis for ON-and OFF-center responses in retinal ganglion cells. *Science* **194**, 193–195 (1976).

91. Nelson, R., Famiglietti, E. V. & Kolb, H. Intracellular staining reveals different levels of stratification for on- and off-center ganglion cells in cat retina. *J. Neurophysiol.* **41**, 472–483 (1978).

92. Peichl, L. Alpha ganglion cells in mammalian retinae: Common properties, species differences, and some comments on other ganglion cells. *Vis. Neurosci.* **7**, 155–169 (1991).

93. Krieger, B., Qiao, M., Rousso, D. L., Sanes, J. R. & Meister, M. Four alpha ganglion cell types in mouse retina: Function, structure, and molecular signatures. *PLOS ONE* **12**, e0180091 (2017).

94. Greschner, M., Thiel, A., Kretzberg, J. & Ammermüller, J. Complex Spike-Event Pattern of Transient on-off Retinal Ganglion Cells. *J. Neurophysiol.* **96**, 2845–2856 (2006).

95. Hattar, S., Liao, H.-W., Takao, M., Berson, D. M. & Yau, K.-W. Melanopsin-Containing Retinal Ganglion Cells: Architecture, Projections, and Intrinsic Photosensitivity. *Science* **295**, 1065–1070 (2002).

96. Gamlin, P. D. R. *et al.* Human and macaque pupil responses driven by melanopsin-containing retinal ganglion cells. *Vision Res.* **47**, 946–954 (2007).

97. Dacey, D. M. *et al.* Melanopsin-expressing ganglion cells in primate retina signal colour and irradiance and project to the LGN. *Nature* **433**, 749–754 (2005).

98. Hattar, S. *et al.* Central projections of melanopsin-expressing retinal ganglion cells in the mouse. *J. Comp. Neurol.* **497**, 326–349 (2006).

99. Troy, J. B., Einstein, G., Schuurmans, R. P., Robson, J. G. & Enroth-Cugell, C. Responses to sinusoidal gratings of two types of very nonlinear retinal ganglion cells of cat. *Vis. Neurosci.* **3**, 213–223 (1989).

100. Sivyer, B., Taylor, W. R. & Vaney, D. I. Uniformity detector retinal ganglion cells fire complex spikes and receive only light-evoked inhibition. *Proc. Natl. Acad. Sci.* **107**, 5628–5633 (2010).

101. Barlow, H. B. & Hill, R. M. Selective Sensitivity to Direction of Movement in Ganglion Cells of the Rabbit Retina. *Science* **139**, 412–412 (1963).

102. Barlow, H. B. & Levick, W. R. The mechanism of directionally selective units in rabbit's retina. *J. Physiol.* **178**, 477–504 (1965).

103. Famiglietti, E. V. Dendritic Co-stratification of ON and ON-OFF directionally selective ganglion cells with starburst amacrine cells in rabbit retina. *J. Comp. Neurol.* **324**, 322–335 (1992).

104. O'Malley, D. M., Sandell, J. H. & Masland, R. H. Co-release of acetylcholine and GABA by the starburst amacrine cells. *J. Neurosci.* **12**, 1394–1408 (1992).

105. Yoshida, K. *et al.* A Key Role of Starburst Amacrine Cells in Originating Retinal Directional Selectivity and Optokinetic Eye Movement. *Neuron* **30**, 771–780 (2001).

106. Briggman, K. L., Helmstaedter, M. & Denk, W. Wiring specificity in the direction-selectivity circuit of the retina. *Nature* **471**, 183–188 (2011).

107. Hubel, D. H. & Wiesel, T. N. Receptive fields of single neurones in the cat's striate cortex. *J. Physiol.* **148**, 574–591 (1959).

108. Hubel, D. H. & Wiesel, T. N. Receptive fields, binocular interaction and functional architecture in the cat's visual cortex. *J. Physiol.* **160**, 106–154 (1962).

109. Maex, R. & Orban, G. A. Model circuit of spiking neurons generating directional selectivity in simple cells. *J. Neurophysiol.* **75**, 1515–1545 (1996).

110. Livingstone, M. S. Mechanisms of Direction Selectivity in Macaque V1. *Neuron* **20**, 509–526 (1998).

111. Lee, S.-H. *et al.* Activation of specific interneurons improves V1 feature selectivity and visual perception. *Nature* **488**, 379–383 (2012).

112. Lien, A. D. & Scanziani, M. Cortical direction selectivity emerges at convergence of thalamic synapses. *Nature* **558**, 80–86 (2018).

113. Cruz-Martín, A. *et al.* A dedicated circuit links direction-selective retinal ganglion cells to the primary visual cortex. *Nature* **507**, 358–361 (2014).

114. Hillier, D. *et al.* Causal evidence for retina-dependent and -independent visual motion computations in mouse cortex. *Nat. Neurosci.* **20**, 960–968 (2017).

115. Rasmussen, R., Matsumoto, A., Dahlstrup Sietam, M. & Yonehara, K. A segregated cortical stream for retinal direction selectivity. *Nat. Commun.* **11**, 831 (2020).

116. Niell, C. M. & Stryker, M. P. Modulation of Visual Responses by Behavioral State in Mouse Visual Cortex. *Neuron* **65**, 472–479 (2010).

117. Fu, Y. *et al.* A Cortical Circuit for Gain Control by Behavioral State. *Cell* **156**, 1139–1152 (2014).

118. Pakan, J. M. *et al.* Behavioral-state modulation of inhibition is context-dependent and cell type specific in mouse visual cortex. *eLife* **5**, e14985 (2016).

119. Jurjut, O., Georgieva, P., Busse, L. & Katzner, S. Learning Enhances Sensory Processing in Mouse V1 before Improving Behavior. *J. Neurosci.* **37**, 6460–6474 (2017).

120. Parker, A., Derrington, A., Blakemore, C., Maunsell, J. H. R. & Cook, E. P. The role of attention in visual processing. *Philos. Trans. R. Soc. Lond. B. Biol. Sci.* **357**, 1063–1072 (2002).

121. Pakan, J. M., Francioni, V. & Rochefort, N. L. Action and learning shape the activity of neuronal circuits in the visual cortex. *Curr. Opin. Neurobiol.* **52**, 88–97 (2018).

122. Führer, D., Zysset, S. & Stumvoll, M. Brain Activity in Hunger and Satiety: An Exploratory Visually Stimulated fMRI Study. *Obesity* **16**, 945–950 (2008).

123. McTeague, L. M., Gruss, L. F. & Keil, A. Aversive learning shapes neuronal orientation tuning in human visual cortex. *Nat. Commun.* **6**, 7823 (2015).

124. Ichida, J. M. & Casagrande, V. A. Organization of the feedback pathway from striate cortex (V1) to the lateral geniculate nucleus (LGN) in the owl monkey (Aotus trivirgatus). *J. Comp. Neurol.* **454**, 272–283 (2002).

125. Angelucci, A. & Sainsbury, K. Contribution of feedforward thalamic afferents and corticogeniculate feedback to the spatial summation area of macaque V1 and LGN. *J. Comp. Neurol.* **498**, 330–351 (2006).

126. Webb, B. S. *et al.* Feedback from V1 and inhibition from beyond the classical receptive field modulates the responses of neurons in the primate lateral geniculate nucleus. *Vis. Neurosci.* **19**, 583–592 (2002).

127. Nahmani, M. & Erisir, A. VGluT2 immunochemistry identifies thalamocortical terminals in layer 4 of adult and developing visual cortex. *J. Comp. Neurol.* **484**, 458–473 (2005).

128. Tamamaki, N. *et al.* Green fluorescent protein expression and colocalization with calretinin, parvalbumin, and somatostatin in the GAD67-GFP knock-in mouse. *J. Comp. Neurol.* **467**, 60–79 (2003).

129. Marshel, J. H., Kaye, A. P., Nauhaus, I. & Callaway, E. M. Anterior-Posterior Direction Opponency in the Superficial Mouse Lateral Geniculate Nucleus. *Neuron* **76**, 713–720 (2012).

130. Grubb, M. S. & Thompson, I. D. Quantitative Characterization of Visual Response Properties in the Mouse Dorsal Lateral Geniculate Nucleus. *J. Neurophysiol.* **90**, 3594–3607 (2003).

131. Dubin, M. W. & Cleland, B. G. Organization of visual inputs to interneurons of lateral geniculate nucleus of the cat. *J. Neurophysiol.* **40**, 410–427 (1977).

132. Famiglietti, E. V. Dendro-dendritic synapses in the lateral geniculate nucleus of the cat. *Brain Res.* **20**, 181–191 (1970).

133. Bickford, M. E., Carden, W. B. & Patel, N. C. Two types of interneurons in the cat visual thalamus are distinguished by morphology, synaptic connections, and nitric oxide synthase content. *J. Comp. Neurol.* **413**, 83–100 (1999).

134. Yoshida, M., Sasa, M. & Takaori, S. Serotonin-mediated inhibition from dorsal raphe nucleus of neurons in dorsal lateral geniculate and thalamic reticular nuclei. *Brain Res.* **290**, 95–105 (1984).

135. Hartveit, E. & Heggelund, P. The effect of acetylcholine on the visual response of lagged cells in the cat dorsal lateral geniculate nucleus. *Exp. Brain Res.* **95**, 443–449 (1993).

136. T, K. & Y, H. Acetylcholine releases of mesopontine PGO-on cells in the lateral geniculate nucleus in sleep-waking cycle and serotonergic regulation. *Prog. Neuropsychopharmacol. Biol. Psychiatry* **20**, 1213–1227 (1996).

137. Mize, R. R. & Payne, M. P. The innervation density of serotonergic (5-HT) fibers varies in different subdivisions of the cat lateral geniculate nucleus complex. *Neurosci. Lett.* **82**, 133–139 (1987).

138. Pasik, P., Pasik, T. & Holstein, G. R. Serotonin-immunoreactivity in the monkey lateral geniculate nucleus. *Exp. Brain Res.* **69**, 662–666 (1988).

139. Ellis, E. M., Gauvain, G., Sivyer, B. & Murphy, G. J. Shared and distinct retinal input to the mouse superior colliculus and dorsal lateral geniculate nucleus. *J. Neurophysiol.* **116**, 602–610 (2016).

140. Reese, B. E. & Jeffery, G. Crossed and uncrossed visual topography in dorsal lateral geniculate nucleus of the pigmented rat. *J. Neurophysiol.* **49**, 877–885 (1983).

141. McLaughlin, T. & O'Leary, D. D. M. Molecular Gradients and Development of Retinotopic Maps. *Annu. Rev. Neurosci.* **28**, 327–355 (2005).

142. Kay, J. N. *et al.* Retinal Ganglion Cells with Distinct Directional Preferences Differ in Molecular Identity, Structure, and Central Projections. *J. Neurosci.* **31**, 7753–7762 (2011).

143. Sherman, S. M. The thalamus is more than just a relay. *Curr. Opin. Neurobiol.* **17**, 417–422 (2007).

144. Crick, F. Function of the thalamic reticular complex: the searchlight hypothesis. *Proc. Natl. Acad. Sci.* **81**, 4586–4590 (1984).

145. McAlonan, K., Cavanaugh, J. & Wurtz, R. H. Guarding the gateway to cortex with attention in visual thalamus. *Nature* **456**, 391–394 (2008).

146. Portas, C. M. *et al.* On-line detection of extracellular levels of serotonin in dorsal raphe nucleus and frontal cortex over the sleep/wake cycle in the freely moving rat. *Neuroscience* **83**, 807–814 (1998).

147. Li, Y. *et al.* Serotonin neurons in the dorsal raphe nucleus encode reward signals. *Nat. Commun.* **7**, 10503 (2016).

148. Lee, M. D., Somerville, E. M., Kennett, G. A., Dourish, C. T. & Clifton, P. G. Tonic regulation of satiety by 5-HT1B receptors in the mouse: converging evidence from behavioural and c-fos immunoreactivity studies? *Eur. J. Neurosci.* **19**, 3017–3025 (2004).

149. Voigt, J.-P. & Fink, H. Serotonin controlling feeding and satiety. *Behav. Brain Res.* **277**, 14–31 (2015).

150. Peters, A., Proskauer, C. C., Feldman, M. L. & Kimerer, L. The projection of the lateral geniculate nucleus to area 17 of the rat cerebral cortex. V. Degenerating axon terminals synapsing with Golgi impregnated neurons. *J. Neurocytol.* **8**, 331–357 (1979).

151. Kondo, S. & Ohki, K. Laminar differences in the orientation selectivity of geniculate afferents in mouse primary visual cortex. *Nat. Neurosci.* **19**, 316–319 (2016).

152. Bullier, J. & Kennedy, H. Projection of the lateral geniculate nucleus onto cortical area V2 in the macaque monkey. *Exp. Brain Res.* **53**, 168–172 (1983).

153. Bienkowski, M. S. *et al.* Extrastriate connectivity of the mouse dorsal lateral geniculate thalamic nucleus. *J. Comp. Neurol.* **527**, 1419–1442 (2019).

154. Tootell, R. B., Hamilton, S. L. & Switkes, E. Functional anatomy of macaque striate cortex. IV. Contrast and magno- parvo streams. *J. Neurosci.* **8**, 1594–1609 (1988).

155. Ries, C. R. & Puil, E. Ionic Mechanism of Isoflurane's Actions on Thalamocortical Neurons. *J. Neurophysiol.* **81**, 1802–1809 (1999).

156. Lein, E. S. *et al.* Genome-wide atlas of gene expression in the adult mouse brain. *Nature* **445**, 168–176 (2007).

157. Goldey, G. J. *et al.* Removable cranial windows for long-term imaging in awake mice. *Nat. Protoc.* **9**, 2515–2538 (2014).

158. Wang, L. & Krauzlis, R. J. Visual Selective Attention in Mice. *Curr. Biol.* **28**, 676-685.e4 (2018).

159. Pologruto, T. A., Sabatini, B. L. & Svoboda, K. ScanImage: flexible software for operating laser scanning microscopes. *Biomed. Eng. Online* **2**, 13 (2003).

160. Pnevmatikakis, E. A. & Giovannucci, A. NoRMCorre: An online algorithm for piecewise rigid motion correction of calcium imaging data. *J. Neurosci. Methods* **291**, 83–94 (2017).

161. Walls, F. L. & Vig, J. R. Fundamental limits on the frequency stabilities of crystal oscillators. *IEEE Trans. Ultrason. Ferroelectr. Freq. Control* **42**, 576–589 (1995).

162. Marvin, J. S. *et al.* An optimized fluorescent probe for visualizing glutamate neurotransmission. *Nat. Methods* **10**, 162–170 (2013).

163. Zingg, B. *et al.* AAV-Mediated Anterograde Transsynaptic Tagging: Mapping Corticocollicular Input-Defined Neural Pathways for Defense Behaviors. *Neuron* **93**, 33–47 (2017).

164. Shanks, J. A. *et al.* Corticothalamic Axons Are Essential for Retinal Ganglion Cell Axon Targeting to the Mouse Dorsal Lateral Geniculate Nucleus. *J. Neurosci.* **36**, 5252–5263 (2016).

165. Silva, A. J. Miniaturized two-photon microscope: seeing clearer and deeper into the brain. *Light Sci. Appl.* **6**, e17104–e17104 (2017).

166. Hoy, J. L., Yavorska, I., Wehr, M. & Niell, C. M. Vision drives accurate approach behavior during prey capture in laboratory mice. *Curr. Biol. CB* **26**, 3046–3052 (2016).

167. Dana, H. *et al.* Sensitive red protein calcium indicators for imaging neural activity. *eLife* **5**, e12727 (2016).